

Negative regulators of plant immunity derived from cinnamyl alcohol dehydrogenases are targeted by multiple *Phytophthora* Avr3a-like effectors

Tingting Li¹ , Qinhu Wang¹ , Ruirui Feng¹, Licai Li¹, Liwen Ding¹, Guangjin Fan¹, Weiwei Li¹, Yu Du¹, Meixiang Zhang¹, Guiyan Huang¹, Patrick Schäfer^{2,3} , Yuling Meng¹, Brett M. Tyler⁴  and Weixing Shan¹ 

¹State Key Laboratory of Crop Stress Biology for Arid Areas and College of Agronomy, Northwest A&F University, Yangling, Shaanxi 712100, China; ²School of Life Sciences, University of Warwick, Gibbet Hill Campus, Coventry, CV4 7AL, UK; ³Warwick Integrative Synthetic Biology Centre, University of Warwick, Coventry, CV4 7AL, UK; ⁴Center for Genome Research and Biocomputing and Department of Botany and Plant Pathology, Oregon State University, Corvallis, OR 97331, USA

Author for correspondence:
Weixing Shan
Tel: +86 029 8708 0102
Email: wxshan@nwfau.edu.cn

Received: 5 June 2019
Accepted: 15 August 2019

New Phytologist (2019)
doi: 10.1111/nph.16139

Key words: Avr3a, CAD7, host target, *Phytophthora*, plant immunity, RXLR effector.

Summary

- Oomycete pathogens secrete numerous effectors to manipulate host immunity. While some effectors share a conserved structural fold, it remains unclear if any have conserved host targets. Avr3a-like family effectors, which are related to *Phytophthora infestans* effector PiAvr3a and are widely distributed across diverse clades of *Phytophthora* species, were used to study this question.
- By using yeast-two-hybrid, bimolecular fluorescence complementation and co-immunoprecipitation assays, we identified members of the plant cinnamyl alcohol dehydrogenase 7 (CAD7) subfamily as targets of multiple Avr3a-like effectors from *Phytophthora* pathogens.
- The CAD7 subfamily has expanded in plant genomes but lost the lignin biosynthetic activity of canonical CAD subfamilies. In turn, we identified CAD7s as negative regulators of plant immunity that are induced by *Phytophthora* infection. Moreover, AtCAD7 was stabilized by Avr3a-like effectors and involved in suppression of pathogen-associated molecular pattern-triggered immunity, including callose deposition, reactive oxygen species burst and WRKY33 expression.
- Our results reveal CAD7 subfamily proteins as negative regulators of plant immunity that are exploited by multiple Avr3a-like effectors to promote infection in different host plants.

Introduction

Oomycetes are eukaryotic microbes that resemble filamentous fungi in morphology and physiology but belong to the kingdom Stramenopila (Tyler, 2001). Oomycetes include many destructive plant pathogens (Kamoun *et al.*, 2015), such as the notorious *Phytophthora infestans*, which caused the Irish potato famine (Haas *et al.*, 2009), and the broad-host-range pathogen *Phytophthora capsica*, which can infect at least 71 species of cultivated plants and weeds representing 27 families of plants, including tomato, pepper, cucurbits and *Nicotiana* species (Granke *et al.*, 2012; Lamour *et al.*, 2012).

Plants have evolved an innate immune system that contains at least two principal overlapping layers of defense (Jones & Dangl, 2006). The first one is pattern-triggered immunity (PTI), which relies on plasma membrane-localized pattern recognition receptors (PRRs) to perceive apoplastic effectors (de Wit, 2016; Wang & Wang, 2018; Wang *et al.*, 2018) and microbe-associated molecular patterns (MAMPs; e.g. the lipid-binding elicitor protein INF1). The second layer of plant immunity relies on the nucleotide-binding domain and leucine-rich repeat (NB-LRR)-

type immune receptors to perceive pathogen effectors within the plant cytoplasm. The latter was formerly known as gene-for-gene resistance and is now termed effector-triggered immunity (ETI) (Flor, 1971; Jones & Dangl, 2006; Boller & He, 2009).

One component of defense responses has been identified as cinnamyl alcohol dehydrogenases (CADs), which contribute to structural lignification during development. In addition, a number of them are strongly induced during infection and are involved in localized lignification as a barrier against infection. In *Arabidopsis*, nine genes have been annotated as encoding CADs (AtCAD1–9) (Costa *et al.*, 2003). Only AtCAD4 and AtCAD5 were confirmed as having significant activity against cinnamyl aldehydes (Kim *et al.*, 2004). *Arabidopsis* double mutants lacking AtCAD4 and AtCAD5 exhibit a limp floral stem with 40% reduction of lignin (Sibout *et al.*, 2005) and also are more susceptible to infection (Tronchet *et al.*, 2010). The close paralogs, AtCAD7 and AtCAD8 (previously called ELI3-1 and ELI3-2), were shown to be strongly induced by pathogens and pathogen-derived elicitors (Kiedrowski *et al.*, 1992). AtCAD8 (ELI3-2) was shown to be preferentially active towards 2-methoxybenzaldehyde, with much weaker activity against 3-methoxybenzaldehyde,

salicylaldehyde, benzaldehyde and cinnamaldehyde (Somssich *et al.*, 1996; Vega-Arreguin *et al.*, 2014). A closely related potato CAD-like protein, DRD-1, was also strongly induced by infection or wounding, and exhibited broad specificity towards aromatic and aliphatic aldehydes with the lowest K_m towards 2-methoxybenzaldehyde, salicylaldehyde and hexanal (Montesano *et al.*, 2003). The preferred substrates of AtCAD1–3, 6 and 9 have not been clearly identified (Kim *et al.*, 2004). On the basis of patterns of tissue-specific gene expression, AtCAD1, 6, 7, 8 and 9 were identified as perhaps contributing in a minor way to developmental lignification, while AtCAD2 and AtCAD3 did not appear to be associated with lignification (Kim *et al.*, 2007).

PiAvr3a and its homologs in *Phytophthora sojae* (PsAvr1b, PsAvh1, PsAvh4 and PsAvh5) and *P. capsici* (PcAvr3a1 to PcAvr3a14) are all Avr3a-like effectors (Shan *et al.*, 2004; Armstrong *et al.*, 2005; Bos, 2007; Jiang *et al.*, 2008) with a similar structure (Boutemy *et al.*, 2011; Win *et al.*, 2012; Sun *et al.*, 2013). *PiAvr3a* contributes to the virulence of *P. infestans* (Armstrong *et al.*, 2005; Bos *et al.*, 2006, 2010). It can suppress two BAK1/SERK3-dependent PTI responses, INF1-triggered cell death (ICD) and flg22-triggered immunity (Chaparro-Garcia *et al.*, 2011, 2015). *PiAvr3a*^{KI} and *PiAvr3a*^{EM} are two alleles of *PiAvr3a*. *PiAvr3a*^{KI} can be recognized by potato resistance protein R3a while *PiAvr3a*^{EM} evades recognition (Armstrong *et al.*, 2005). To date, two host targets of PiAvr3a have been reported. One is a host E3 ubiquitin ligase, CMPG1, which is required for ICD and stabilized by PiAvr3a^{KI} (Bos *et al.*, 2010). The second is the plant GTPase Dynamin-related protein 2 (DRP2), which is involved in immune receptor-mediated endocytosis and required for FLS2 internalization (Chaparro-Garcia *et al.*, 2015). Recently we found that PcAvr3a12, an Avr3a-like effector from *P. capsici*, could enhance *Arabidopsis* susceptibility to *P. capsici* and specifically target the host peptidyl-prolyl *cis-trans* isomerase FKBP15-2 to suppress endoplasmic reticulum-mediated plant immunity (Fan *et al.*, 2018). Although this indicates the diversity of host proteins targeted by Avr3a-like effectors, it remains largely unknown whether they also have common targets.

In the present study, we found that Avr3a-like effectors are widely distributed across the genus *Phytophthora*. We screened for host proteins targeted by multiple *Phytophthora* Avr3a-like effectors, and found that related CAD-like proteins from *Arabidopsis thaliana* (AtCAD7) and *Nicotiana benthamiana* (NbCAD7) interacted with Avr3a-like effectors from *P. capsici*, *P. infestans* and *P. sojae*. Furthermore, we found evidence that both AtCAD7 and NbCAD7 could act as negative regulators of plant innate immunity, and that this activity does not require the putative enzyme active site residues of these proteins.

Materials and Methods

Strains and plant materials

Agrobacterium GV3101 was used for transient expression, stable transformation and virus-induced gene silencing (VIGS) experiments. *Saccharomyces cerevisiae* strains AH109 and Y187 were used for yeast transformation and mating. For inoculation in *Arabidopsis*, oomycete pathogen *P. capsici* strain LT263 was used.

For *Arabidopsis* transformation, wild-type Col-0 was used. *Agrobacterium*-mediated transformation was performed as previously described (Zhang *et al.*, 2006). All plants were grown at 23°C under a 13 h : 11 h, light : dark cycle.

Plasmid construction

For over-expression, the entire open reading frames of *AtCADs* were amplified by PCR and cloned into pART27 (Gleave, 1992) with *KpnI* and *Clal*. For our bimolecular fluorescence complementation assay (BiFC), the new GATEWAY vectors (Gehl *et al.*, 2009) were used. For yeast-two-hybrid assays (Y2H), all effectors (without signal peptide) were amplified by PCR and cloned into pGBKT7 while *AtCAD* family members were cloned into pGADT7. To generate VIGS constructs, a 300 bp fragment of *NbCAD7* was amplified from *N. benthamiana* cDNA and cloned into the binary vector pTRV2, while TRV2::GFP was constructed as a control. All constructs were sequenced at GenScript (Nanjing, China). All primers used for plasmid constructions are listed in Supporting Information Table S1.

Yeast-two-hybrid assay

To screen for the effector targets, a cDNA library was prepared with the infected *Arabidopsis* leaves using *Phytophthora parasitica* strain Pp016 at 2 d post-infiltration. Y2H screening was performed using the Matchmaker Gal4 Two-Hybrid System 3 (Clontech, Palo Alto, CA, USA) as described in the manual.

Bimolecular fluorescence complementation assay

BiFC was performed using protocols described previously (Gehl *et al.*, 2009). We used the binary vectors pDEST-G^WVYNE, pDEST-VYNE(R)^{GW}, pDEST-G^WVYCE and pDEST-VYCE(R)^{GW}. These vectors were transiently expressed in *N. benthamiana* and fluorescence was observed 3 d after agroinfiltration.

Co-immunoprecipitation assay (Co-IP)

The proteins of *N. benthamiana* leaves expressing Co-IP constructs were extracted at 3 d after agroinfiltration, using lysis buffer (25 mM Tris-HCl pH 7.5, 150 mM NaCl, 1 mM EDTA and 0.5% NP-40) plus 2% (w/v) polyvinylpyrrolidone (PVPP), 1 mM dithiothreitol (DTT) and a protease inhibitor cocktail (Biotool). The total protein was incubated at 4°C for 3 h with GFP-Trap_A beads (Chromotek, Planegg-Martinsried, Germany). The beads were then washed with dilution buffer (10 mM Tris-HCl pH 7.5, 150 mM NaCl and 0.5 mM EDTA). The resuspended GFP-Trap_A beads were boiled for 10 min at 95°C to dissociate the immunocomplexes.

Western blotting

To detect BiFC proteins, the samples were extracted using lysis buffer (50 mM Tris-HCl pH 7.5, 150 mM NaCl, 1 mM EDTA, 1% TritonX-100, 1% sodium deoxycholate, 5 mM

sodium fluoride and 1 mM sodium orthovanadate), plus 2% (w/v) PVPP, 5 mM DTT and a protease inhibitor cocktail. For stabilization experiments, the samples were extracted using lysis buffer (25 mM Tris-HCl pH 7.5, 150 mM NaCl, 1 mM EDTA and 0.5% NP-40) plus 2% (w/v) PVPP, 1 mM DTT and a protease inhibitor cocktail. Sodium dodecyl sulfate–polyacrylamide gel electrophoresis (SDS-PAGE) was performed with proteins. Antibodies (anti-HA, anti-Myc, anti-FLAG, anti-mCherry, anti-GFP, goat anti-mouse and anti-rabbit) were used according to descriptions given in the manual.

Transient expression analysis

Agrobacterium transient expression assays were carried out on 4–6-wk-old *N. benthamiana*. The agroinfiltration medium consisted of 10 mM MgCl₂, 10 mM MES and 150 mM acetosyringone. *Agrobacterium* strain GV3101 with final OD₆₀₀ values of 0.2–0.4 in agroinfiltration medium was used. Transient expression assays in *Arabidopsis* protoplasts were performed as described (Yoo *et al.*, 2007).

qRT-PCR analysis

For all reverse transcriptase PCR (RT-PCR) analysis, cDNA was synthesized with PrimeScript RT reagent Kit with gDNA Eraser (TaKaRa, Shiga, China), and PCRs were performed with FastStart Universal SYBR Green Master according to the manufacturer's instructions (Roche). *AtUBC9* was used as a reference gene in *Arabidopsis* for normalization. *NbEF1α* was used as a reference gene in *N. benthamiana* for normalization. All primers used for quantitative RT-PCR (qRT-PCR) are listed in Table S1.

VIGS analysis

VIGS was performed using a previously described method (Liu *et al.*, 2002). For *NbCAD7* silencing, a 300 bp fragment of *NbCAD7* was designed using the SGN VIGS tool (Fernandez-Pozo *et al.*, 2015) to ensure both efficiency and specificity of silencing. The *NbCAD7* fragment was cloned into TRV2 and a TRV2 vector containing a *GFP* fragment was used as a control. To choose the proper leaves for the following analysis, *PDS*-silenced plants were used to monitor the silencing effect. Infiltration of agrobacterium cultures containing TRV1 and TRV2 was performed on the lower leaves of six-leaf stage *N. benthamiana*. The agroinfiltration media of TRV1 and TRV2 were mixed in 1 : 1 ratio and a final concentration of OD₆₀₀ = 0.3 was used. The VIGS plants were used for further analysis 3–5 wk after infiltration.

Inoculation analysis

For *Arabidopsis* inoculation, c. 800–1200 zoospores prepared from *P. capsici* strain LT263 were used to infect the 4 wk old leaves. For *N. benthamiana* inoculation, 0.3 cm² mycelium plugs cut from the *P. capsici* strain LT263 cultures, or c. 800 zoospores

prepared from *P. infestans* strain Pc21336 (a lab strain isolated in China, virulent on R3 plants) were used to infect the VIGS plants.

Confocal microscopy

Imaging was conducted on an Olympus FV1000 confocal microscope using HCX APO L 10×/0.4, 20×/0.75 and 40×/0.95 water-dipping lenses. Green and yellow fluorescent protein (GFP and YFP) were excited at 488 nm and detected at 500–540 nm. For mCherry observation, fluorescence was excited at 559 nm and detected at 580–630 nm.

Histochemical analysis

Two-month-old *Arabidopsis* stems were used for histochemical analysis. The basal part of the stem was sectioned by hand and then stained. Wiesner and Maule reactions were performed according to standard protocols (Sibout *et al.*, 2005).

Callose deposition and ROS burst analyses

Four-week-old *Arabidopsis* leaves treated with 1 μM flg22 were used for all analyses. Both callose deposition and reactive oxygen species (ROS) burst were assayed as previously described (Luna *et al.*, 2011; Sang & Macho, 2017).

Sequence and phylogenetic analysis

To identify the Avr3a-like sequences in oomycetes (Dataset S1), PiAvr3a, PsAvr1b, PsAvh5, PcAvr3a4, PcAvr3a11 and PcAvr3a12 were used to search the oomycete genomes via tBLASTN with an E-value cut-off of e-20. To identify the CAD homologs in plants (Dataset S2), AtCAD1–9 were used to search the plant proteins via BLASTP with an E-value cut-off of e-25. The protein sequences were aligned with M-COFFEE (Wallace *et al.*, 2006) (Avr3a-like) or CLUSTALW2 (Larkin *et al.*, 2007) (CAD), and the phylogenetic relationships were inferred by PHYML (Guindon *et al.*, 2010). The trees were visualized by FIGTREE (<http://tree.bio.ed.ac.uk/software/figtree>).

Results

Avr3a-like proteins are distributed widely across the genus *Phytophthora*

To gain a comprehensive view of the distribution of Avr3a-like proteins in oomycetes, we used the sequences of the effectors PiAvr3a (Armstrong *et al.*, 2005; Bos *et al.*, 2006, 2010), PsAvr1b (Shan *et al.*, 2004; Dou *et al.*, 2008), PsAvh5 (Sun *et al.*, 2013), PcAvr3a4 (Yaeno *et al.*, 2011), PcAvr3a11 (Boutemy *et al.*, 2011) and PcAvr3a12 (Fan *et al.*, 2018) to search oomycete genomes available in GenBank using tBLASTN with an E-value cutoff of e-20. One to 14 sequence matches were observed in the genomes of 10 surveyed species representing clades 1, 2, 4, 7, 8 and 10 (Kroon *et al.*, 2012) in *Phytophthora* (Fig. 1a). No

sequence matches with an E-value better than e^{-20} were observed outside the genus *Phytophthora*, including downy mildews, *Phytophthora* and *Pythium* species. A phylogenetic tree of the Avr3a-like protein sequences (Fig. 1b) revealed two broad subfamilies, one containing PsAvh5, and the other containing PiAvr3a, PsAvr1b and the three *P. capsici* proteins used as queries. The Avh5 subfamily contained members from all *Phytophthora* species except *P. kernoviae*, while the PiAvr3a-PsAvr1b subfamily was missing representatives from *P. brassicae*, *P. ramorum* and *P. cinnamomi*. Large species-specific gene family expansions have occurred in *P. capsici* (10 members), *P. megakarya* (six members) and *P. palmivora* (five members), while smaller expansions (two to four members) have occurred in *P. infestans*, *P. sojae* and *P. kernoviae*. All the Avr3a-like genes in *P. capsici*, except *PcAvr3a16*, *PcAvr3a17* and *PcAvr3a18*, were organized in a single 187 kb cluster within the PacBio assembly of LT263 (Fig. S1), indicating that they may have arisen from tandem duplication events.

We used qRT-PCR to assay the transcript levels of *PcAvr3a1*, *PcAvr3a3*, *PcAvr3a5*, *PcAvr3a6*, *PcAvr3a11*, *PcAvr3a12* and *PcAvr3a14* relative to *PcActin*-like genes during leaf infection of its host plants *Arabidopsis* and *N. benthamiana*. (Fig. S2). The results revealed that *PcAvr3a14* exhibited the highest transcript levels during early infection of *Arabidopsis* leaves (up to 100% of *PcActin* levels at 3–6 h post-infection (hpi)), while *PcAvr3a3* showed the highest transcript levels during early infection of *N. benthamiana* leaves, up to 350% of *PcActin* at 3 hpi. *PcAvr3a5* exhibited moderate transcript levels during *Arabidopsis* infection (up to 10% of *PcActin* over 3–12 hpi) while *PcAvr3a1*, *PcAvr3a5*, *PcAvr3a12* and *PcAvr3a14* exhibited moderate transcript levels during *N. benthamiana* infection (up to 80% of *PcActin* over 3–24 hpi). Transcripts of *PcAvr3a6* and *PcAvr3a11* could barely be detected during infection of either plant.

Multiple *Phytophthora* Avr3a-like effectors interact with AtCAD7

Given the structural conservation and partial sequence conservation of Avr3a-like effectors in *Phytophthora* spp. (Figs 1, S3) we examined if there were host proteins targeted by multiple Avr3a family members. We screened a cDNA library prepared from *Phytophthora parasitica*-infected *Arabidopsis* leaves with PiAvr3a^{KI} and PsAvr1b using a Y2H assay. Our analysis (Fig. 2a) revealed that both PiAvr3a^{KI} and PsAvr1b interacted with AtCAD7. We thus hypothesized that AtCAD7 might be targeted by other Avr3a-like effectors. To test this hypothesis, we examined the interactions of AtCAD7 with several other Avr3a-like effectors, including PiAvr3a^{EM}, PcAvr3a1 and PcAvr3a12 (PcAvr3a12a) by pairwise Y2H. Consistently, all these effectors interacted with AtCAD7 in the Y2H assay while the non-Avr3a-like RXLR effector PITG_23129 from *P. infestans* did not (Fig. 2a).

To retest the interactions in plant cells, we used BiFC assays. The effectors (PsAvr1b, PiAvr3a^{KI}, PiAvr3a^{EM}, PcAvr3a1, PcAvr3a12, and the control PITG_23129) were fused with the N-terminal fragment of YFP (YFP^N) and AtCAD7 was fused with the C-terminal fragment of YFP (YFP^C). All these YFP

fragment-fused proteins were successfully expressed as verified by western blotting (Fig. S4). Confocal microscopy revealed that the Avr3a-like effectors fused to YFP^N and AtCAD7 fused to YFP^C complemented to produce YFP fluorescence in *N. benthamiana* (Fig. 2b), while the control PITG_23129 did not (Fig. 2b). These results suggested that AtCAD7 could bind to the Avr3a-like effectors *in planta*.

We next extended the examination of Avr3a family proteins to PcAvr3a3, PcAvr3a5, PcAvr3a6, PcAvr3a11 and PcAvr3a14, using Y2H and BiFC assays (Fig. 3a,b). Both the Y2H and the BiFC assays indicated interactions of AtCAD7 with PcAvr3a3, PcAvr3a5 and PcAvr3a6. However, PcAvr3a11 and PcAvr3a14 showed weak or inconsistent evidence, respectively, for interactions with AtCAD7.

We then used Co-IP assays to further validate the interactions of the PcAvr3a-like proteins with AtCAD7. Myc-tagged AtCAD7 was co-expressed in *N. benthamiana* with GFP fusions of each PcAvr3a-like proteins, the effector proteins were then recovered onto GFP-Trap A beads, and the presence of AtCAD7 was determined by western blotting with anti-Myc antibodies. The results (Fig. 3c) confirmed strong interactions of AtCAD7 with PcAvr3a1, PcAvr3a6 and PcAvr3a12. PcAvr3a11 showed no interaction while PcAvr3a3, PcAvr3a5 and PcAvr3a14 showed weaker interactions.

The CAD7 subfamily is expanded in plant genomes

Because *N. benthamiana* is a host for *P. capsici* and also for *P. infestans*, we were interested to determine whether CAD7 proteins from *N. benthamiana* could be bound by Avr3a-like effectors from these two pathogens. We first conducted a genome-wide analysis to determine the distribution of CAD7 homologs in the genomes of *N. benthamiana* and other plant species. As expected (Boerjan *et al.*, 2003), we found that CAD family proteins were conserved from moss to higher land plants. The proteins were distributed into five clades (Fig. S5). The *Arabidopsis* CADs fell into four of the clades, with AtCAD4 and 5 together, AtCAD2, 3 and 9 together, AtCAD6, 7 and 8 together, and AtCAD1 alone.

Interestingly, we observed that the CAD7 subfamily, containing AtCAD6, 7 and 8, was expanded in several plant genomes (Fig. S5). The CAD7 subfamily has eight members in rice, four in maize, eight in poplar, three in *Arabidopsis*, seven in soybean, 15 in *N. benthamiana*, nine in potato, seven in tomato and four in pepper. By contrast, in the *N. benthamiana* genome, non-CAD7 clades comprised only six members in total. Multiple co-orthologs of AtCAD7 and 8 were encoded in *N. benthamiana* (marked with blue dots in Fig. S5). These co-orthologs grouped into six subclades (7c1 to 7c6). Using bidirectional-best BLAST searches and ORTHOMCL (Li *et al.*, 2003), we identified NbCAD7 (Niben101Scf02907g06016.1) in clade 7c1 as the closest ortholog of AtCAD7 and 8.

As *AtCAD7* and *AtCAD8* were reported to be induced by bacterial and by fungal elicitors (Schmelzer *et al.*, 1989; Kiedrowski *et al.*, 1992; Trezzini *et al.*, 1993), we tested whether transcript levels of *AtCAD7*, *AtCAD8* and also *AtCAD6* were elevated

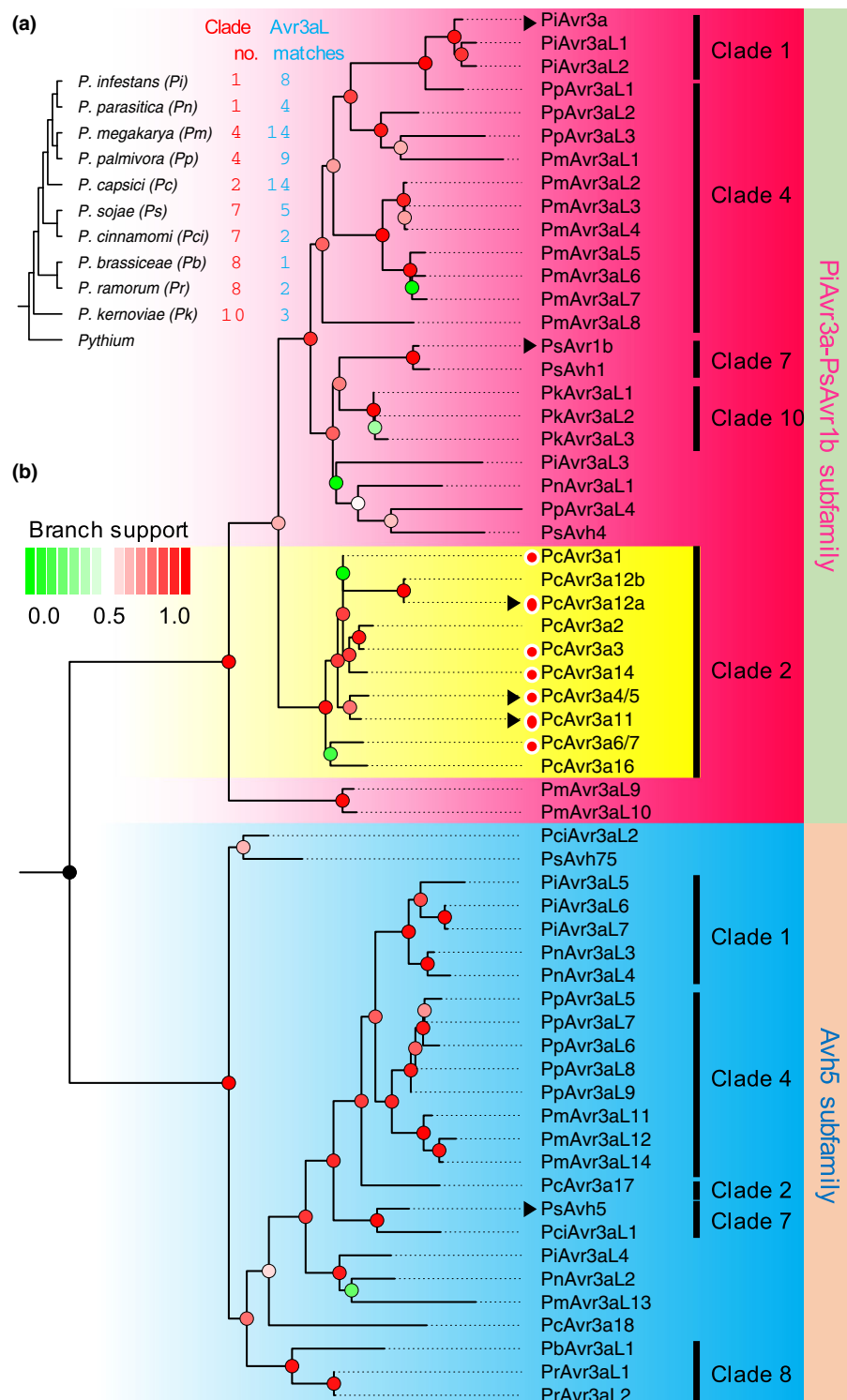


Fig. 1 Avr3a-like effectors are distributed widely across *Phytophthora* species. (a) The number of Avr3a-like (Avr3aL) sequence matches in the genome of 10 surveyed *Phytophthora* species. The phylogeny is based on a previous description of the genus *Phytophthora* (Kroon *et al.*, 2012). (b) Phylogenetic analysis of Avr3a-like effectors in the genus *Phytophthora*. The Avr3a-like effectors that specifically expanded in *P. capsici* are highlighted in yellow. The six query sequences are indicated by black triangles, and the PcAvr3a-like effectors further characterized in this study are indicated by red circles. The phylogenetic relationship was inferred by PHYLML based on an alignment generated with M-COFFEE. Color key (from green to red) indicates the approximate likelihood ratio test and Shimodaira–Hasegawa (aLRT SH)-like branch support value, from low to high. Black dot marks the root of the phylogenetic tree.

during oomycete infection. Using qRT-PCR, we observed that *AtCAD6* levels were increased just under four-fold at 12 hpi, *AtCAD7* transcripts were elevated over four-fold by 24 hpi, and *AtCAD8* transcripts were elevated over five-fold by 60 hpi (Fig. S6a–c). These observations were reinforced by using transgenic *Arabidopsis* plants carrying the beta-glucuronidase gene (*GUS*) driven by the promoters of *AtCAD6*, 7 and 8 (Fig. S6d–f).

Thus, transcripts of all three *Arabidopsis* genes in the *CAD7* clade appeared to be moderately increased by *P. capsici* infection.

Because *AtCAD6* and *AtCAD8* transcript levels were elevated during infection along with *AtCAD7*, and share sequence similarity with *AtCAD7*, we used a Y2H assay to test *AtCAD6* and *AtCAD8* proteins for interactions with PcAvr3a1, PcAvr3a3, PcAvr3a11 and PcAvr3a12. The results suggested that *AtCAD6*

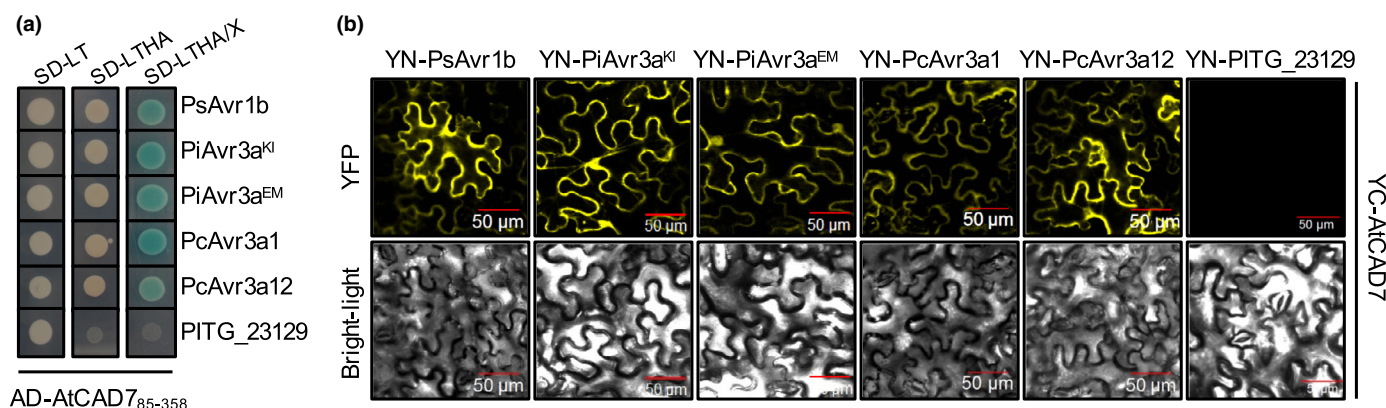


Fig. 2 Multiple *Phytophthora* Avr3a-like effectors interact with CAD7. (a) *Arabidopsis thaliana* CAD7 (AtCAD7) interacts with Avr3a-like effectors as determined by a Y2H assay. AtCAD7₈₅₋₃₅₈ on pGADT7 (AD) vector, which was derived from cDNA library screening, was used to confirm the interactions with effectors (PsAvr1b, PiAvr3a^{KI}, PiAvr3a^{EM}, PcAvr3a1, PcAvr3a12 and PITG_23129) cloned into pGBKT7 (BD). Yeast transformants were separately transferred onto SD/-Leu/-Trp (SD-LT), SD-Leu/-Trp/-His/-Ade (SD-LTHA), and SD/-Leu/-Trp/-His/-Ade medium with 40 µg ml⁻¹ X-α-gal (SD-LTHA/X). The growth of yeast transformants on SD-LT medium demonstrated successful transformations. The growth of yeast transformants on SD-LTHA (His and Ade reporter genes activated) and blue color on SD-LTHA/X (LacZ reporter gene activated) indicate interactions. Pictures were taken after 3 d of culture. (b) AtCAD7 interacts with Avr3a-like effectors in the BiFC assay. The effectors fused with the N terminus of YFP and AtCAD7 fused with the C terminus of YFP were transiently co-expressed in *Nicotiana benthamiana* and examined by confocal microscopy at 3 d post-infiltration (dpi). The complementation of fluorescence indicates interaction between assayed proteins. The candidate RXLR effector PITG_23129 from *P. infestans* served as a control.

could interact with PcAvr3a12, but that AtCAD8 could not interact with any of the four effectors (Fig. S7).

Targeting of NbCAD7 by *P. capsici* and *P. infestans* Avr3a-like effectors

To test if *N. benthamiana* co-orthologs of AtCAD7 could interact with Avr3a-like effectors from *P. capsici* and *P. infestans*, we selected NbCAD7 as a representative co-ortholog and used Y2H, BiFC and Co-IP assays to test its interactions with the effectors. While the BiFC assays suggested that NbCAD7 might interact with all of the effectors tested (Fig. 3d,g), only the interactions of NbCAD7 with PcAvr3a12 and PiAvr3a^{EM} were confirmed by both Co-IP (Fig. 3f,h) and Y2H (Fig. 3e,i). PiAvr3a^{KI} showed a weak interaction by Co-IP and none by Y2H (Fig. 3e,i).

To investigate whether the CAD7 proteins and Avr3a-like effectors exhibited similar subcellular distributions, we co-expressed GFP-AtCAD7 and GFP-NbCAD7 with mCherry-PcAvr3a1 and mCherry-PcAvr3a12, respectively, in *N. benthamiana*. All fusion proteins were expressed and intact in plant cells as determined by western blotting (Fig. S8a). Confocal microscopy showed that both mCherry-PcAvr3a1 and mCherry-PcAvr3a12 showed the same distributions in the cytoplasm and nucleus of plant cells as the two GFP-CAD7 proteins (Fig. S8b,c). Thus, the distributions of the CAD7 and Avr3a-like effector proteins were consistent with the possibility that they interact with each other.

Silencing of AtCAD7 and NbCAD7 attenuates *Phytophthora* infection

To explore the function of the AtCAD7 gene during *P. capsici* infection, we analyzed *Arabidopsis* T-DNA insertion mutant lines of AtCAD7. Unfortunately, RT-PCR verification showed

that the T-DNA insertion in the promoter of AtCAD7 (SALK_083037C) did not affect AtCAD7 expression (data not shown). We therefore silenced AtCAD7 in *Arabidopsis* stable RNAi lines. Two silenced lines, Ri.1 and Ri.2, showed 97% and 76% silencing of AtCAD7, based on qRT-PCR assays (Fig. 4a) whereas the transcript levels of AtCAD6, AtCAD8 and AtCAD5 were not significantly affected (Fig. S9a–c). Neither Ri.1 nor Ri.2 showed any phenotypic defects in growth (Fig. S10a). When inoculated with *P. capsici*, the lesions at 2 d post-infiltration (dpi) were slightly (20%) but significantly ($P < 0.001$) smaller on the RNAi plants as compared to the wild type Col-0 (Fig. 4b,c).

To test the function of NbCAD7 during *P. capsici* and *P. infestans* infection of *N. benthamiana*, we silenced NbCAD7 using VIGS. Due to the high sequence similarity among the co-orthologs of NbCAD7, it was difficult to silence NbCAD7 exclusively. To minimize off-target silencing, a 300 bp fragment of NbCAD7 was designed using the SGN VIGS tool (Fernandez-Pozo *et al.*, 2015). Nevertheless, after agroinfiltration, qRT-PCR examination showed that NbCAD7 (Fig. 4d) and also the three closest paralogs in clade 7c1, NbCAD1, NbCAD2 and NbCAD5 (Fig. S9d–f), were silenced in plants expressing TRV::NbCAD7 (*tNb7*) as compared to plants expressing the control TRV::GFP (*tGFP*) construct. By contrast, NbCAD18, the ortholog of AtCAD5, was unaffected (Fig. S9g). The *tNb7* plants showed a decreased growth rate as compared to control *tGFP* plants (Fig. S10b). Trypan blue staining showed that both *P. capsici* and *P. infestans* colonization in the *tNb7* leaves was noticeably reduced, as compared to the control *tGFP* leaves (Fig. 4e–f). The *P. capsici* lesion diameters were slightly (9%) but significantly ($P < 0.05$) smaller in leaves expressing TRV::NbCAD7 as compared to the *tGFP* control (Fig. 4g), while the *P. infestans* lesions were 47% smaller ($P < 0.001$) (Fig. 4h). Taken together, these

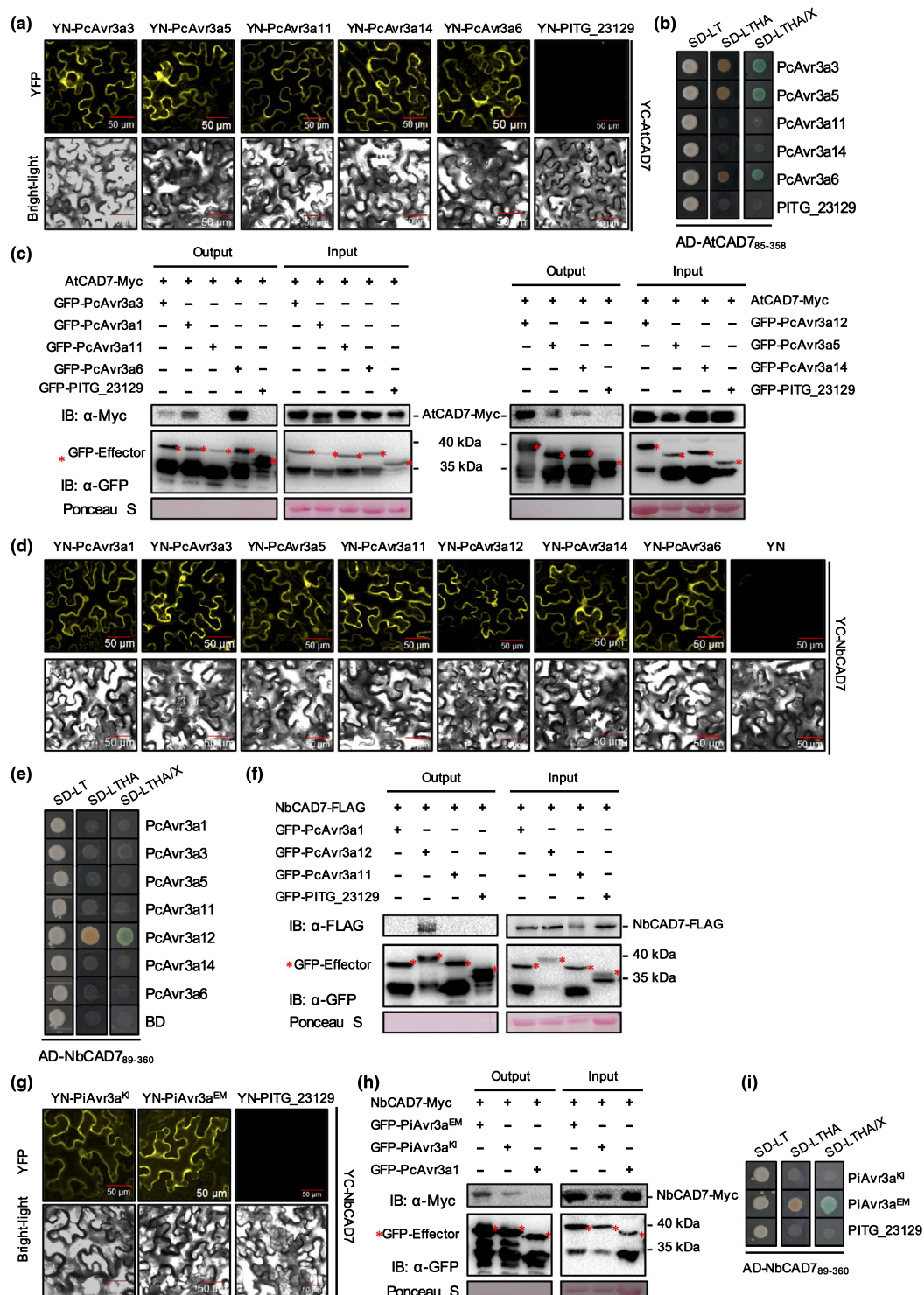


Fig. 3 Host CAD7s are conserved targets of *Phytophthora* Avr3a-like effectors. (a–c) AtCAD7 interacts with Avr3a-like effectors from *P. capsici* in BiFC (a), Y2H (b) and Co-IP (c) assays. The proteins used for Co-IP were derived from *Nicotiana benthamiana* co-expressed AtCAD7-Myc with GFP-PcAvr3a1, GFP-PcAvr3a3, GFP-PcAvr3a11, GFP-PcAvr3a6, GFP-PcAvr3a12, GFP-PcAvr3a5, GFP-PcAvr3a14 and GFP-PITG_23129. Total proteins were then subjected to incubation with GFP-Trap_A beads and anti-Myc (α -Myc) immune blotting of the output was used to identify the co-immunoprecipitation of AtCAD7-Myc with GFP-effectors. (d–f) *Nicotiana benthamiana* CAD7 (NbCAD7) interacts with Avr3a-like effectors from *P. capsici* in BiFC (d), Y2H (e) and Co-IP (f) assays. In Co-IP assays, NbCAD7-FLAG was co-expressed with GFP-PcAvr3a1, GFP-PcAvr3a12, GFP-PcAvr3a128 and GFP-PITG_23129. Anti-FLAG (α -FLAG) immune blotting of the output was used to identify the co-immunoprecipitation of NbCAD7-FLAG with GFP-effectors. (g–i) NbCAD7 interacts with Avr3a-like effectors from *P. infestans* in BiFC (g), Co-IP (h) and Y2H (i) assays. In Co-IP assays, NbCAD7-Myc was co-expressed with GFP-PiAvr3a^{EM}, GFP-PiAvr3a^{KI}, and GFP-PcAvr3a1. Anti-Myc immune blotting of the output was used to identify the co-immunoprecipitation of NbCAD7-Myc with GFP-effectors. The complete proteins of GFP-effectors are marked with red asterisks. Note that all these Co-IP assays are qualitative rather than quantitative experiments.

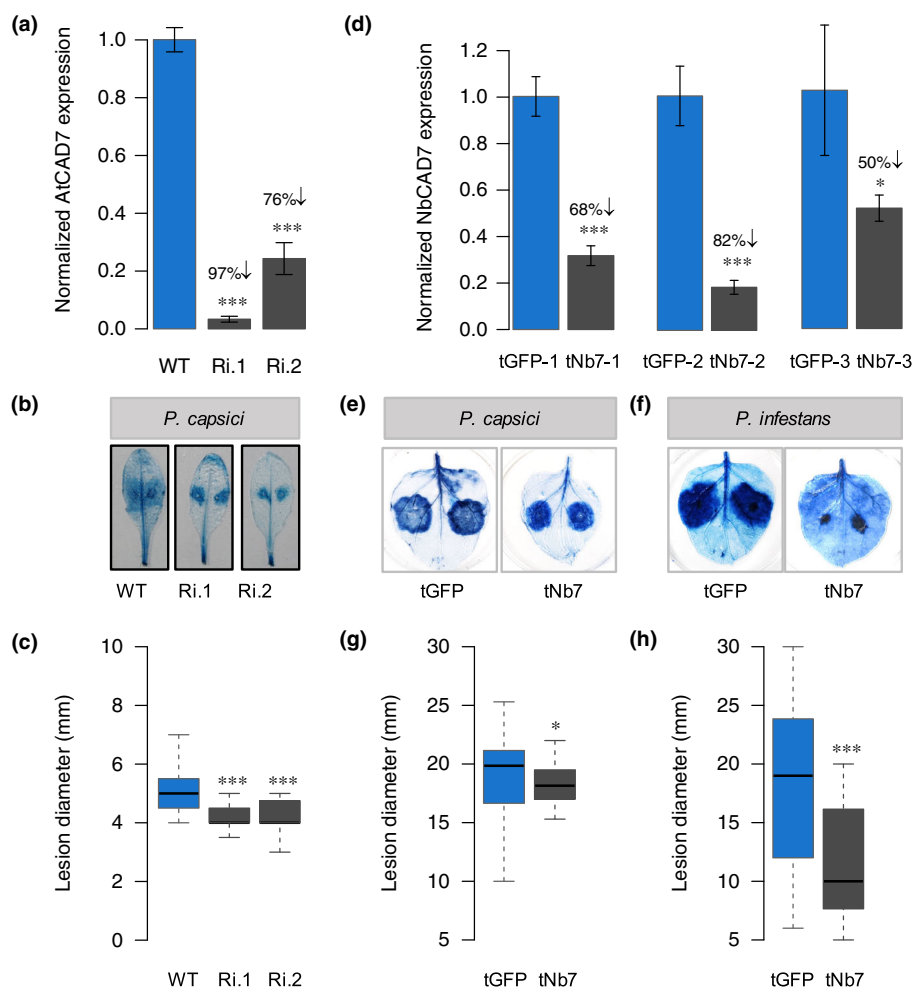


Fig. 4 Silencing of *CAD7* enhances resistance against *Phytophthora*. (a–c) Silencing of *AtCAD7* decreased the colonization of *P. capsici* in *Arabidopsis*. (a) *AtCAD7* is down-regulated in two independent RNAi lines (Ri.1 and Ri.2) compared with that of the wild type Col-0 (WT). Total RNA extracted from Ri.1, Ri.2 and the WT plants was used for quantification of *AtCAD7* transcripts by qRT-PCR. Constitutively expressed *AtUBC9* was used as a reference gene. Error bars represent the standard deviations from three individual transgenic plants derived from each independent transformation line. (b) Trypan blue staining showed that the colonization of *P. capsici* in Ri.1 and Ri.2 leaves was decreased as compared to that in WT. (c) Statistical analyses of the lesion diameters of *P. capsici* infection in the WT and RNAi plants at 2 d post-inoculation. (d–h) Silencing of *NbCAD7* decreased the colonization of *P. capsici* and *P. infestans* in *Nicotiana benthamiana*. (d) Statistical analyses of qRT-PCR results showed that *NbCAD7* was down-regulated by 50–82% in TRV::*NbCAD7* (*tNb7*) plants as compared to the TRV::GFP (*tGFP*) plants. Total RNA extracted from *N. benthamiana* expressing TRV::*NbCAD7* and TRV::GFP at 4 wk after infiltration was used for qRT-PCR. Constitutively expressed *NbEF1α* was used as a reference gene. Three biological replicates were independently derived from VIGS plants and each replicate contained six leaves from three VIGS plants (two leaves from each plant) in the same batch. Error bars represent the standard deviations from three individual VIGS plants. Trypan blue staining showed that the lesions caused by *P. capsici* (e) and *P. infestans* (f) that developed in *N. benthamiana* leaves expressing TRV::*NbCAD7* were smaller than that in the control leaves expressing TRV::GFP. The inoculations were performed 4 wk after agro-infiltration with TRV constructs. *Phytophthora capsici* infections were observed at 2 d post-inoculation and *P. infestans* infections were observed at 8 d post-inoculation. Boxplots showing the statistical analyses of lesion diameters in *tNb7* and *tGFP* leaves infected by *P. capsici* (g) and *P. infestans* (h). Each boxplot illustrates lesion diameters measured from > 10 leaves from the same batch; each inoculation test was repeated at least four times with similar results. In (c, g, h), the upper quartile, median and lower quartile are shown in each box, while the bars outside the box indicate the 5th and 95th percentiles. In (a, c, d, g, h), one-sided *t*-tests were used to assess significance: *, $P < 0.05$; ***, $P < 0.001$.

results suggested that *CAD7* silencing in *Arabidopsis* and *N. benthamiana* slightly reduced susceptibility against *P. capsici* and *P. infestans*.

Overexpression of *AtCAD7* in *Arabidopsis* enhances *P. capsici* colonization

To further examine the function of *AtCAD7* during *Phytophthora* infection, we next overexpressed *AtCAD7* in *Arabidopsis*. After

qRT-PCR screening, two independent lines (OE7.7 and OE7.9) with significant elevation of *AtCAD7* transcript levels (Fig. 5a) were selected for further analyses. Neither line showed developmental phenotypes compared to the wild type (WT) plants (Fig. S10c). Inoculation tests with *P. capsici* showed that pathogen colonization was increased in OE7 plants as compared to WT (Fig. 5b) and *P. capsici* lesion diameters in OE7 leaves were 38% larger ($P < 0.01$) than those in WT plants (Fig. 5c). Concordantly, qPCR results indicated that the *P. capsici* biomass

was significantly ($P < 0.001$) increased in OE7 plants, 3.6-fold in the case of OE7.7 (Fig. 5d). Taken together with the data from the *AtCAD7* silencing plants, these results suggested that *AtCAD7* supports *Phytophthora* infection and may function as a negative regulator of plant defense against *P. capsici*.

By contrast to *AtCAD7*, transient over-expression of NbCAD7 in *N. benthamiana* leaves did not result in a significant increase in *P. capsici* lesion size (Fig. S11), perhaps because the leaves already produced an over-abundance of NbCAD proteins.

Mutations in the predicted enzyme activity sites of *AtCAD7* do not abolish its supportive function in *P. capsici* infection

Although *AtCAD7* has a very low enzymatic activity *in vitro* towards cinnamyl aldehydes as compared to *AtCAD5* (Kim *et al.*, 2004), its close paralog, *AtCAD8*, does have substantial activity towards 2-methoxybenzaldehyde (Somssich *et al.*, 1996). To test whether the predicted enzymatic activity sites of *AtCAD7* were necessary for its interactions with Avr3a-like effectors and its negative role in plant defense against *Phytophthora*, we generated plants carrying two independent mutations (Fig. 6a) that abolish two different sets of key residues predicted to be required for enzyme activity (Bomati & Noel, 2005; Youn *et al.*, 2006) (Fig. S12). *AtCAD7m1* (*AtCAD7*^{C46A, T48A, S51A}) abolishes residues predicted to be required for the binding of catalytic Zn²⁺, NADP⁺ and substrates, while *AtCAD7m2* (*AtCAD7*^{S210A, T211A, S212A, K215A}) disrupted the predicted NADP⁺-binding residues of *AtCAD7*. BiFC assays showed that both mutants interacted with PcAvr3a5, PcAvr3a12 and PcAvr3a14 as observed with WT *AtCAD7* (Fig. 6b,c). Co-IP assays confirmed that *AtCAD7m2* interacted with all three Avr3a-like effectors (Fig. 6d) as observed for WT *AtCAD7* (Fig. 3c) (i.e. strongly with PcAvr3a12, and weakly with PcAvr3a5 and PcAvr3a14). We thus conclude that the predicted key enzyme activity sites of *AtCAD7* are not required for its interactions with the tested Avr3a-like effectors.

We next generated *Arabidopsis* lines expressing *AtCAD7m1* (OE7m1) or *AtCAD7m2* (OE7m2) (Fig. 6e) driven by the 35S promoter. Similar to OE7, OE7m1 and OE7m2 plants did not show any phenotypic changes in development (Fig. S10c). Neither set of mutations noticeably altered the ability of *AtCAD7* over-expression to increase susceptibility to *P. capsici* infection (Fig. 6f–h). Thus, we conclude that the ability of *AtCAD7* to promote *P. capsici* infection does not require its putative enzymatic activity.

To analyze the contribution of *AtCAD7* to lignification in *Arabidopsis*, we performed lignin staining with the sectioned stems of *AtCAD7*-silenced *Arabidopsis* lines Ri.1 and Ri.2. Both Wiesner (Fig. S13a) and Maule (Fig. S13b) staining reactions showed that stem xylems of Ri plants had staining patterns similar to the WT plants. This confirmed earlier studies on the minor function of *AtCAD7* in lignification (Kim *et al.*, 2004, 2007) and indicated that *AtCAD7* silencing had no noticeable impact on xylem lignification. In addition, we also stained the inflorescence stems of the *Arabidopsis* over-expression lines, OE7 and OE7m, with the WT plants as controls. Consistently, the dye intensities and staining patterns of all xylem tissues visualized by the Wiesner (Fig. S13c) and Maule (Fig. S13d) reactions did not show any differences. We thus conclude that the contribution of *AtCAD7* to lignin biosynthesis is, at most, minor (Kim *et al.*, 2004).

NbCAD7 amplifies the suppression of INF1-triggered cell death by PiAvr3a^{KI}

Given that PiAvr3a^{KI} could suppress INF1-triggered plant immunity (Bos *et al.*, 2006), we performed cell death assays in *NbCAD7*-silenced plants (*tNb7*) and control plants (*tGFP*) to investigate the role of NbCAD7 in INF1-triggered immunity. To measure the severity of cell death more precisely, we defined three cell death grades for treated *N. benthamiana* leaves (Fig. 7a). Constructs carrying *INF1* were agroinfiltrated into

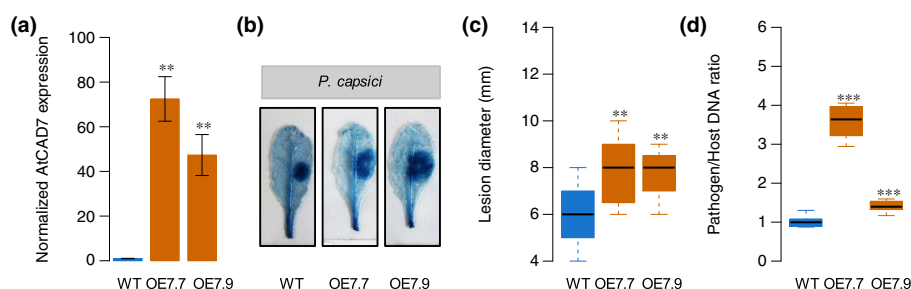
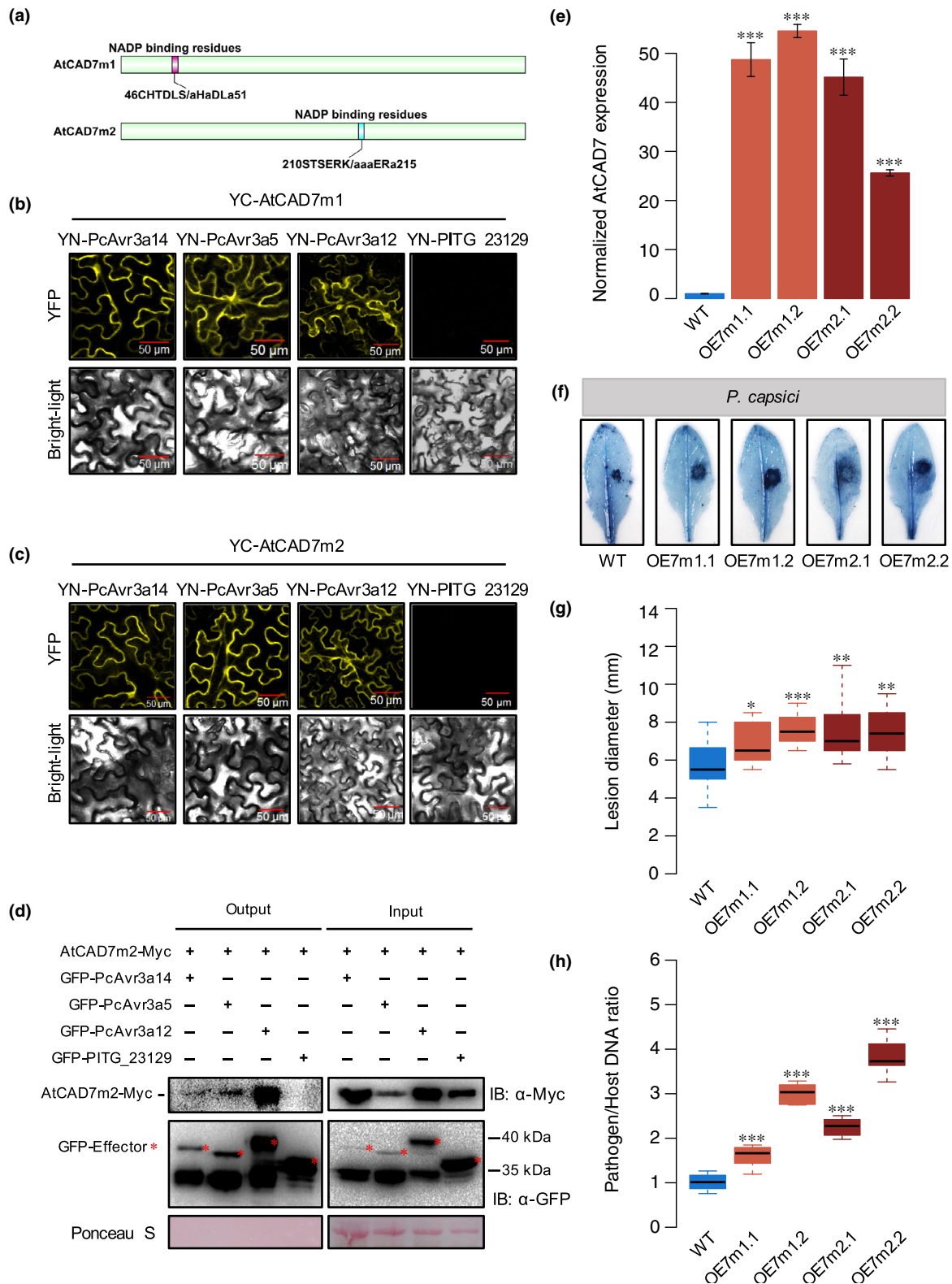


Fig. 5 Overexpression of *AtCAD7* decreases resistance against *Phytophthora capsici*. (a) *AtCAD7* is up-regulated in two independent overexpression lines (OE7) compared with wild-type Col-0 (WT) in the absence of infection. Constitutively expressed *AtUBC9* was used as a reference gene. Error bars represent the standard deviations from three individual transgenic plants derived from each independent transformation line. (b) Trypan blue staining showed that colonization by *P. capsici* increased in OE7 as compared to WT. (c) Statistical analyses of the lesion diameters of *P. capsici* infection in the WT and OE7 plants at 2 d post-infiltration (dpi). Each boxplot illustrates the lesion diameters measured from at least 10 leaves. The experiment was repeated at least four times with similar results. (d) Statistical analyses of *P. capsici* biomass in the infected leaves of the WT and OE7 plants. The biomass was measured as the ratio of the pathogen DNA relative to the host plant DNA as determined by qPCR. *Phytophthora capsici* ACTIN (*PcACTIN*) and *Arabidopsis* *UBC9* (*AtUBC9*) were used as reference genes in qPCR analyses. The biomass in the WT plants was set to 1. Each boxplot summarizes the biomass measured from six individuals. The leaves of 4-wk old *Arabidopsis* were inoculated with zoospores of *P. capsici* strain LT263. In (c, d), the upper quartile, median and lower quartile are shown in each box, while the bars outside the box indicate the 5th and 95th percentiles. In (a, c, d), one-sided *t*-tests were used to assess significance: **, $P < 0.01$; ***, $P < 0.001$.



N. benthamiana plants which had previously been inoculated with *tNb7* and *tGFP* constructs, and the cell death occurrence was recorded. ICD appeared in *tNb7* leaves but not in *tGFP* leaves at 2 dpi (Fig. 7b). Statistical analyses indicated that cell

death triggered by INF1 was significantly ($P < 0.001$) increased in *tNb7* plants as compared to control plants *tGFP* (Fig. 7c) at 2 dpi. This result suggested that ICD was accelerated by silencing of *NbCAD7*. We thus concluded that *NbCAD7* can suppress

Fig. 6 Mutations in the predicted enzyme activity sites of AtCAD7 do not affect its function as a negative regulator of plant immunity or its interaction with Avr3a-like effectors. (a) Overview of two AtCAD7 mutants (AtCAD7m1 and AtCAD7m2) that were mutated at the enzyme activity sites. (b, c) Both AtCAD7m1 and AtCAD7m2 interacted with Avr3a-like effectors in the BiFC assay. PITG_23129 was used as a control. (d) AtCAD7m2 interacted with Avr3a-like effectors in Co-IP assays. The proteins used for Co-IP were derived from *Nicotiana benthamiana* co-expressing AtCAD7m2-Myc with GFP-PcAvr3a14, GFP-PcAvr3a5, GFP-PcAvr3a12 and GFP-PITG_23129. Total proteins were then subjected to incubation with GFP-Trap_A beads and anti-Myc (α -Myc) immune blotting of the output was used to identify the co-immunoprecipitation of AtCAD7-Myc with GFP-effectors. The complete proteins of GFP-effectors are marked with red asterisks. (e) AtCAD7 is up-regulated in OE7m1 and OE7m2 plants compared with that of the wild type Col-0 (WT). Total RNA extracted from OE7m1.1, OE7m1.2, OE7m2.1, OE7m2.2 and the WT plants was used for quantification of AtCAD7 transcripts by qRT-PCR. Constitutively expressed *AtUBC9* was used as a reference gene. Error bars represent the standard deviations from three individual transgenic plants of each independent transformation line. (f) Trypan blue staining showed that the colonization of *Phytophthora capsici* in OE7m1 and OE7m2 leaves increased compared with that in the WT. (g) Statistical analysis indicates that the lesion diameters in OE7m1 and OE7m2 leaves were significantly larger than in the WT. OE7m1 and OE7m2 represent the transgenic *Arabidopsis* lines expressing AtCAD7 mutants. All leaves were challenged with zoospores of *P. capsici* LT263 and the phenotypes were observed at 2 d post-infiltration (dpi). The experiments were repeated three times with similar results. (h) Statistical analyses of the *P. capsici* biomass in the infected leaves of the WT (Col-0) and OE7m plants. The biomass was measured as the ratio of the pathogen DNA relative to the host plant DNA as determined by qPCR. *Phytophthora capsici* ACTIN (*PcACTIN*) and *Arabidopsis UBC9* (*AtUBC9*) were used as reference genes in qPCR analysis. Biomass of the WT plants was set to 1. Each boxplot summarizes the biomass measured from six individuals. In (g, h), the upper quartile, median and lower quartile are shown in each box, while the bars outside the box indicate the 5th and 95th percentiles. In (e, g, h), one-sided *t*-tests were used to assess significance: *, $P < 0.05$; **, $P < 0.01$; ***, $P < 0.001$.

ICD. To further confirm this, we performed cell death assays in *N. benthamiana* leaves transiently overexpressing *NbCAD7* (Nb7OE) and in control leaves expressing *GFP* (GFP). Consistent with the results described above, cell death triggered by INF1 was attenuated in Nb7OE leaves as compared to the GFP leaves at 3 dpi (Fig. 7d,e). These results support that NbCAD7 can negatively regulate ICD. As shown in Fig. S14, transient expression of *AtCAD7* in *N. benthamiana* leaves could also negatively regulate ICD, and this ability was not significantly affected by mutations in the predicted enzyme active site of AtCAD7.

Based on the above results, we hypothesized that *NbCAD7* might modulate the suppression of ICD by *PiAvr3a*^{KI}. To test this hypothesis, constructs containing either *PiAvr3a*^{KI} or control *GFP* were co-expressed with *INF1* in *NbCAD7*-silenced plants (*tNb7*) and control plants (*tGFP*). Cell death was scored at 3 dpi. The results showed that *PiAvr3a*^{KI} suppressed 83% of the ICD in *tGFP* control plants, but to a significantly lesser extent (35%) in *tNb7* plants (Fig. 7f). This indicated that the suppression of ICD by *PiAvr3a*^{KI} was attenuated in *NbCAD7*-silenced plants. Therefore, our results revealed that the ability of *PiAvr3a*^{KI} to suppress ICD was correlated with the transcript levels of *NbCAD7*.

AtCAD7 can suppress callose deposition, ROS burst and WRKY33 expression

Considering that NbCAD7 could suppress ICD, we further examined the ability of *AtCAD7* to modulate innate immunity in *Arabidopsis*. Callose deposition in the plant cell wall is an important barrier against pathogen attack and is a hallmark of PTI triggered by MAMP molecules such as flg22 (Luna *et al.*, 2011). Treatment of *AtCAD7*-overexpression lines (OE7.7 and OE7.9) and *AtCAD7*-silencing lines (Ri.1 and Ri.2) with flg22 showed that callose deposition in leaves was significantly reduced in OE7 leaves and increased in Ri leaves as compared to WT (Fig. 7g). We also analyzed ROS levels, which represents an early PTI response (Baxter *et al.*, 2014; Mittler, 2017), using DAB staining. The analysis showed that in contrast to the ROS burst in WT plants, a reduced oxidative burst was observed in *AtCAD7*-

overexpression lines while an increased burst was observed in *AtCAD7*-silencing lines (Fig. 7g). Statistical analyses across multiple leaves revealed that both callose deposition and ROS levels were significantly reduced in *AtCAD7*-overexpression lines but were enhanced in *AtCAD7*-silencing lines (Fig. 7h,i). To investigate if the expression of defense-related genes was affected by *AtCAD7* overexpression, we performed qRT-PCR assays (Fig. S15). This analysis revealed that among all PTI genes tested, *WRKY33*, a transcription factor gene involved in PTI signaling and defense against necrotrophs (Zheng *et al.*, 2006), showed greatly reduced transcript levels in *Arabidopsis* plants overexpressing *AtCAD7*. Taken together, these results indicated that *AtCAD7* could suppress PTI responses.

AtCAD7 is stabilized by *PiAvr3a* and *PcAvr3a12*

The stability of several host targets of oomycete RXLR effectors is associated with the 26S proteasome (Bos *et al.*, 2010; Wang *et al.*, 2015). To explore whether Avr3a-like effectors could affect accumulation of AtCAD7 and whether the accumulation of AtCAD7 is modulated by the 26S proteasome, *A. tumefaciens* carrying constructs encoding Myc-tagged AtCAD7 was co-infiltrated into *N. benthamiana* along with *A. tumefaciens* carrying constructs encoding GFP-tagged *Avr3a*^{EM}, *Avr3a*^{KI}, *PcAvr3a12* or a GFP control. 26S proteasome inhibitor MG132 or control dimethyl sulfoxide (DMSO) was injected at 36 h after agroinfiltration (hai) and samples were harvested at 48 hai. In the absence of MG132, AtCAD7 showed increased accumulation in the effector-expressing leaves as compared to GFP-expressing leaves (Fig. 8). However, in the presence of MG132, effector expression did not affect AtCAD7 accumulation (Fig. 8). These results suggest that the effectors may increase the accumulation of AtCAD7 by inhibiting 26S proteasome-mediated degradation of AtCAD7. The increased AtCAD7-Myc protein accumulation in the effector-expressing plants was not due to an increased level of the RNA transcript (Fig. 8).

To further confirm the stabilization of AtCAD7 by Avr3a effectors in *Arabidopsis*, we examined AtCAD7-Myc accumulation in the presence and absence of Avr3a effectors in *Arabidopsis*

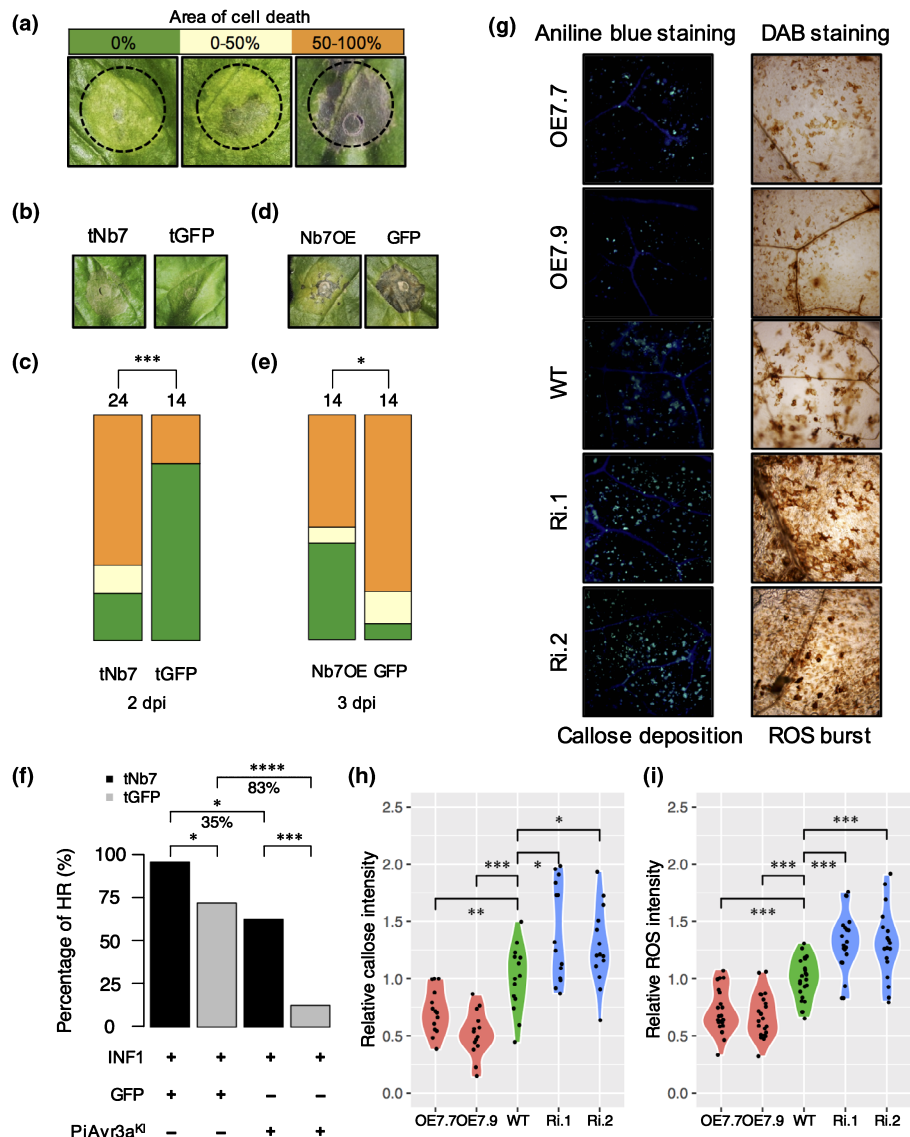
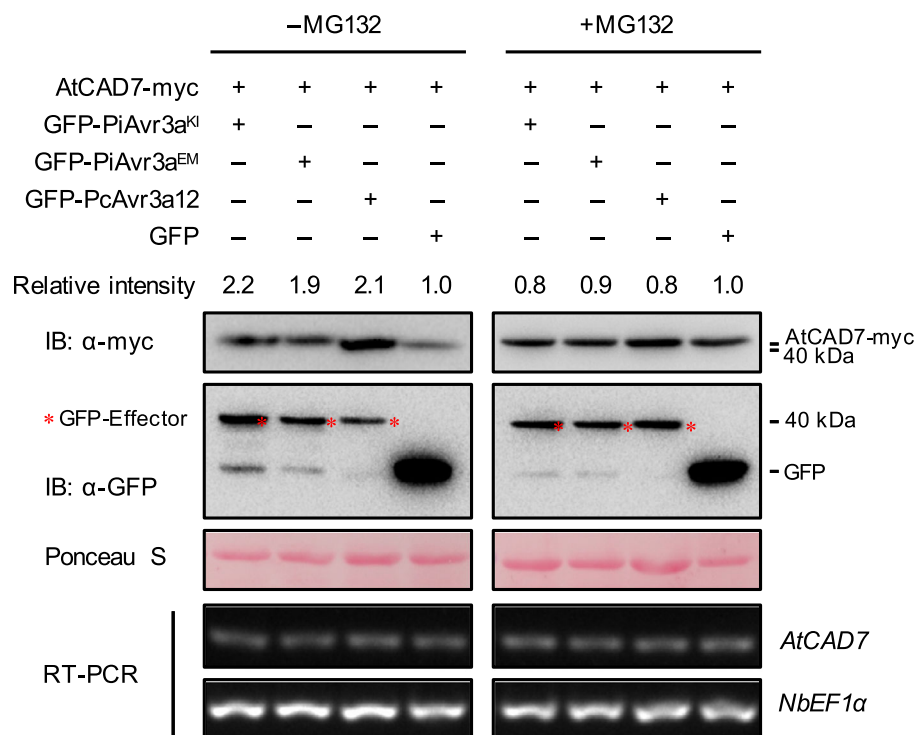


Fig. 7 CAD7 suppresses PTI in the host plant. (a) Three different levels of plant cell death are defined according to the percentage of the cell death area developed in the infiltration area. (b, c) Phenotypes (b) and statistical analyses (c) of plant cell death triggered by INF1 in *Nicotiana benthamiana* expressing TRV::NbCAD7 (*tNb7*) and TRV::GFP (*tGFP*) indicate that silencing of NbCAD7 promotes ICD specifically. (d, e) Phenotypes (d) and statistical analyses (e) of the plant cell death triggered by INF1 in *N. benthamiana* overexpressing NbCAD7 and GFP indicate that overexpression of NbCAD7 attenuates ICD. In (c) and (e), cell death was observed from their first appearance; statistical analyses were based on the most representative stage of the cell death as indicated at the bottom of each column. The differences of cell death in the *N. benthamiana* leaves were assessed by one-sided Wilcoxon rank-sum tests. Numbers above the columns indicate the total number of infiltration sites used for statistical analyses. (f) Silencing of NbCAD7 attenuates the ability of PiAvr3a to suppress ICD. The ability of PiAvr3a to suppress ICD is compromised in *tNb7* plants as compared to control *tGFP* plants. Percentages indicate the inhibition efficiency of PiAvr3a^{Kl} to suppress ICD in *tNb7* plants and *tGFP* plants at 3 d post-infiltration (dpi). The differences of cell death percentage in *N. benthamiana* leaves were assessed using a Fisher's exact test. Each experiment was repeated at least three times with highly similar results. (g) Aniline blue and DAB staining assays show callose deposition and ROS burst, respectively. *Arabidopsis* leaves from AtCAD7-overexpression lines (OE7), AtCAD7-silencing lines (Ri) and the wild-type Col-0 (WT) were treated with 1 μ M flg22 before staining. (h) Violin plot showing the relative intensity of callose deposition from multiple leaves of *Arabidopsis*. (i) Violin plot showing the relative intensity of ROS burst from multiple leaves of *Arabidopsis*. In (h, i), the intensities were quantified by the number of callose or ROS-corresponding pixels and were normalized with the intensities in WT, and one-sided *t*-tests were used to assess significances. In (c, e, f, h, and i): *, $P < 0.05$; **, $P < 0.01$; ***, $P < 0.001$; ****, $P < 0.0001$.

protoplasts. The result clearly showed that AtCAD7-Myc abundance was increased by PiAvr3a and PcAvr3a12 (Fig. S16). We also performed stabilization experiments with NbCAD7 in *N. benthamiana* but did not observe significantly increased NbCAD7 accumulation by Avr3a-like effectors.

Because it was previously identified that PiAvr3a targets and stabilizes the E3 ligase CMPG1 (Bos *et al.*, 2010), we examined if NbCAD7 interacted with NbCMPG1 directly. Both Y2H and BiFC assays showed that there was no direct interaction between them (Fig. S17a,b), suggesting an independent interaction of

Fig. 8 AtCAD7 is stabilized by Avr3a-like effectors in a 26S proteasome-dependent manner. Proteins were derived from *Nicotiana benthamiana* plants co-expressing AtCAD7-Myc and GFP-PiAvr3a^{KI}, GFP-PiAvr3a^{EM}, GFP-PcAvr3a12 or the control (GFP) at 2 d post *Agrobacterium* infiltration. Proteasome inhibitor MG132 or control dimethyl sulfoxide (DMSO, i.e. -MG132) was infiltrated 12 h before harvest. Total proteins were extracted and subjected to SDS-PAGE, followed by anti-Myc (α -Myc) immunodetection of AtCAD7-Myc in the absence or presence of MG132. The recombinant fusion proteins of GFP-effectors are marked with red asterisks. Protein loading is shown by Ponceau S staining. RT-PCR assays for AtCAD7 expression in *N. benthamiana* were performed to ensure equal levels of RNA transcripts. *NbEF1 α* was used an internal control.



PiAvr3a with NbCAD7 and NbCMPG1. Also, PcAvr3a12 is unlikely to interact with NbCMPG1a or NbCMPG1b, as revealed by Y2H and BiFC (Fig. S17c,d).

Discussion

Phytophthora spp. possess a large number of RXLR effectors, which are fast evolving due to selection pressure imposed by the co-evolutionary conflict between pathogens and hosts (Dangl & Jones, 2001; Jones & Dangl, 2006). Despite the diversity of RXLR effectors, several families of effectors show substantial conservation across widely divergent species, including families defined by PsAvh238 (Wang *et al.*, 2011), PsAvh163 (Anderson *et al.*, 2012), HaAvh23/PsAvh73 (Deb *et al.*, 2018) and especially PiAvr3a (Bos, 2007; Vega-Arreguin *et al.*, 2014). The conservation of Avr3a-like effectors, across at least six *Phytophthora* clades, including the highly divergent *P. kernoviae*, suggests a particular significance for this family for pathogenicity on diverse hosts.

Here, we have shown, using Y2H, BiFC and Co-IP assays, that several Avr3a-like effectors from *P. capsici* directly target the protein AtCAD7 in *Arabidopsis* and its closest homolog in *N. benthamiana*, NbCAD7 (Figs 2, 3). PiAvr3a has been previously shown to target the E3-ligase CMPG1 (Bos *et al.*, 2010) as well as the GTPase DRP2 (Chaparro-Garcia *et al.*, 2015). Furthermore, PcAvr3a12 has been shown to bind to AtFKBP15-2 to suppress endoplasmic reticulum-mediated plant immunity (Fan *et al.*, 2018). Our results here showed that NbCMPG1 did not bind to either NbCAD7 or PcAvr3a12, while PiAvr3a did not bind to FKBP15-2 (Fan *et al.*, 2018). Thus, both PiAvr3a and PcAvr3a12 are revealed to have both shared and specific targets in host plants. These observations also suggest that individual

oomycete RXLR effectors may have multiple physiologically relevant host target proteins. Mukhtar *et al.* (2011) also noted numerous examples of effectors from the oomycete *Hyaloperonospora arabidopsidis* and the bacteria *Pseudomonas syringae* that bound multiple *Arabidopsis* target proteins in a Y2H screen.

Our phylogenetic analysis revealed that the CAD7 subfamily of cinnamaldehyde dehydrogenases, defined by AtCAD6, AtCAD7 and AtCAD8, has greatly expanded compared to the other CAD subfamilies. Of these *AtCAD7* (*Eli3-1*) and *AtCAD8* (*Eli3-2*), as well as a parsley homolog, were previously reported to be strongly induced by *P. sojae* elicitors (Gleave, 1992; Trezzini *et al.*, 1993) and by *Pseudomonas* infection (Kiedrowski *et al.*, 1992). Furthermore, *StuCAD6* (*DRD-1*), a closely related potato CAD gene, was reported to be strongly induced during *Erwinia* infection of potato (Montesano *et al.*, 2003). Our data showed, likewise, that *AtCAD6*, *AtCAD7* and *AtCAD8* transcript levels were strongly elevated during *P. capsici* infection of *Arabidopsis* leaves, albeit with different timing (Fig. S6). *AtCAD7* transcript levels exceeded *AtCAD6* levels at all time points (Fig. S6), suggesting that *AtCAD7* represented the most important response to early infection. Of the three tested AtCAD proteins, only AtCAD6 and AtCAD7 (but not AtCAD8) were targeted by PcAvr3a-like proteins, thus suggesting that the early-induced AtCADs are the primary targets for PcAvr3a-like proteins. However, we cannot rule out that AtCAD8 (and other AtCAD proteins) might be targeted by other *P. capsici* RXLR effectors, including other PcAvr3a-like proteins that were not analyzed here.

Although cinnamaldehyde dehydrogenases are typically considered to function in lignin production, our data indicate that

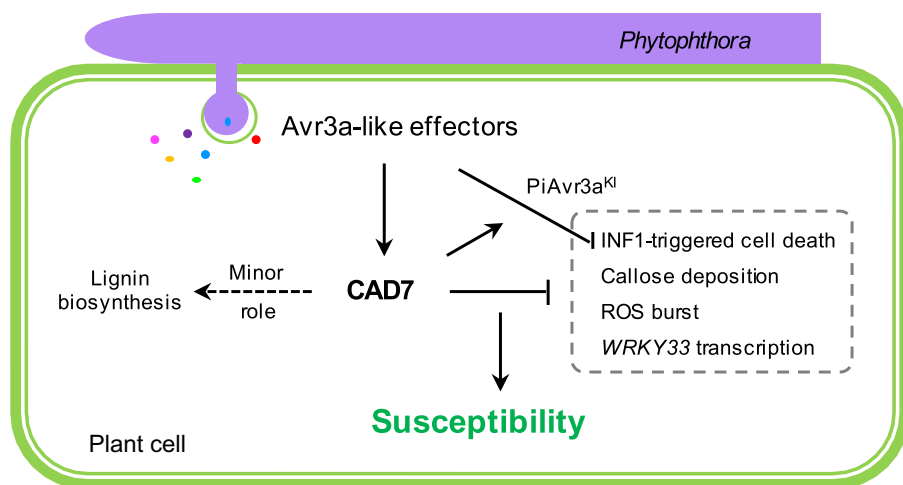


Fig. 9 Proposed model for the role of CAD7 in the negative regulation of plant immunity. Multiple Avr3a-like effectors target and stabilize CAD7, which suppresses PTI as indicated by the suppression of INF1-triggered cell death, callose deposition, ROS burst and WRKY33 transcription. The PTI suppression renders plants susceptible to pathogen infection. During evolution, CAD7 diversification was driven by interactions with *Phytophthora* pathogens, being frequently exploited as a susceptibility factor targeted by pathogen effectors. Colored circle dots represent multiple Avr3a-like effectors.

the CAD7 subfamily proteins primarily have roles as negative regulators of plant immunity. Silencing or over-expression of *AtCAD7* in *Arabidopsis* plants did not discernibly affect lignification (Fig. S13) but made the plants more resistant (Fig. 4) or susceptible (Fig. 5) to *P. capsici*, respectively. Similarly, silencing of *NbCAD7* made *N. benthamiana* leaves more resistant to *P. capsici* and especially to *P. infestans* (Fig. 4), while over-expression did not produce a measurable increase in *P. capsici* lesion size under the conditions of the assay (Fig. S11). The deposition of callose and production of ROS were decreased significantly in the *AtCAD7*-overexpressed plants treated with PTI inducer flg22, while they were significantly increased in the *AtCAD7*-silenced plants (Fig. 7). Most strikingly, the transcript levels of the transcription factor *WRKY33* were reduced 3–4-fold in *Arabidopsis* plants over-expressing *AtCAD7* (Fig. S15). *WRKY33* is a key transcription factor required for resistance of *Arabidopsis* against necrotrophs. It is involved in PTI signaling and defense against necrotrophs (Zheng *et al.*, 2006). Consistent with this, an *N. benthamiana* homolog of *WRKY33*, *WRKY8*, is required for resistance against *P. infestans* and *Botrytis cinerea* (Ishihama *et al.*, 2011).

The negative regulatory role of the CAD7 proteins seems counterintuitive, given their strong induction during infection. However, the induction of negative regulators during a defense response provides a mechanism to modulate or spatially restrict that response (Rodriguez *et al.*, 2016). Furthermore, Hillmer *et al.* (2017) showed via a systems approach that negative feedback loops within plant defense signaling networks provide extensive buffering against interference by pathogen effectors (Tyler, 2017). Thus, pathogen effectors that target CADs to attack lignin biosynthesis might inadvertently stimulate defense if they also target CAD7 sub-family proteins; in this context, the CAD7 sub-family proteins could be considered decoys. Intriguingly however, *P. capsici* and *P. infestans* appears to have evolved Avr3a-like effectors that can exploit this negative feedback loop to the advantage of the pathogen, highlighting once again the relentless nature of the pathogen-plant arms race.

Our data show that over-expression of *NbCAD7* in *N. benthamiana* leaves could partially, but significantly, suppress

ICD, while silencing of *NbCAD7* could accelerate ICD. Silencing of *NbCAD7* could also significantly reduce the suppression of ICD by PiAvr3a^{KI}. However, our data do not support the hypothesis that binding to *NbCAD7* mediates the ability of PiAvr3a^{KI} to suppress ICD. For example, both PcAvr3a12 and PiAvr3a^{EM} interact with *NbCAD7* more strongly in the Y2H assays than PiAvr3a^{KI}, yet neither effector can suppress ICD. Thus, we speculate that PiAvr3a^{KI} and *NbCAD7* suppress ICD additively, or possibly synergistically, through different pathways. These observations are consistent with the finding that the binding of PiAvr3a^{KI} to a different target, CMPG1, is required for suppression of ICD (Bos *et al.*, 2010). On the other hand, we cannot rule out the possibility that the nature of the PiAvr3a^{KI}–*NbCAD7* interaction is different than the interaction of *NbCAD7* with the other Avr3a-like effectors. For example, the *Arabidopsis* RIN4 protein is a conserved target of bacterial effectors AvrB, AvrRPM1 and AvrRpt2, but while AvrB and AvrRPM1 induce phosphorylation of RIN4 (Mackey *et al.*, 2002), AvrRpt2 induces its post-transcriptional disappearance (Mackey *et al.*, 2003).

AtCAD7 and also *AtCAD1*, *AtCAD6*, *AtCAD8* and *AtCAD9* were previously reported to make, at most, minor contributions to lignification (Kim *et al.*, 2007), which is supported by our observations (Fig. S13). *AtCAD8*, which is closely similar to *AtCAD7*, was reported to exhibit 2-methoxybenzaldehyde dehydrogenase activity (Somssich *et al.*, 1996), as was *StuCAD6* (DRD-1) (Montesano *et al.*, 2003). Furthermore, the two closest homologs of *AtCAD7* in cucumber, *CsCAD3* and *CsCAD4*, also preferred 2-methoxybenzaldehyde as a substrate (Varbanova *et al.*, 2011). Thus, *AtCAD7* and *NbCAD7* might also exhibit 2-methoxybenzaldehyde dehydrogenase activity. However, our data indicate that the predicted active site residues of *AtCAD7* are not required for its negative regulation of immunity. We speculate that this dual role of the *AtCAD7* and *NbCAD7* proteins may serve to coordinate immune function with lignification in lignifying tissues, perhaps to redirect the products of the phenylpropanoid pathway away from defense compounds.

The mechanism(s) by which Avr3a-like effectors exploit the negative regulatory function of CAD7 proteins to inhibit defense

are not yet fully clear. Our data showed that over-expression of PiAvr3a^{KI}, PiAvr3a^{EM} or PcAvr3a12 could stabilize co-expressed AtCAD7 protein in *N. benthamiana* leaves and *Arabidopsis* protoplasts, by inhibiting degradation through the 26S proteasome (Figs 8, S16). However, co-expressed NbCAD7 protein was not detectably stabilized in a similar experiment. It is possible that the Avr3a-like effectors do indeed act to stabilize CAD7 proteins, but that features of the assay, including especially the presence of an abundance of endogenous NbCAD7-subfamily proteins, may obscure the full extent of the stabilization. On the other hand, it is plausible that binding of the effectors activates CAD7 function via other mechanisms, for example by stabilizing the binding of CAD7 to the target that it negatively regulates, or by displacing CAD7 from an inhibitor protein.

In summary, the Avr3a-like effectors could target and exploit CAD7, a negative regulator of plant innate immunity, to facilitate pathogen infection by suppressing plant PTI (Fig. 9).






Acknowledgements

We are grateful to Dr Ming-Bo Wang, Dr Jim Peacock and Dr Liz Dennis (CSIRO Agriculture and Food, Canberra, Australia), Dr Francine Govers (Wageningen University, The Netherlands), and all the lab members for their insightful discussions in this study. This work was supported by China Agriculture Research System (CARS-09), National Natural Science Foundation of China (31125022 and 31561143007), the Programme of Introducing Talents of Innovative Discipline to Universities (project 111) from the State Administration of Foreign Experts Affairs (no. B18042), BBSRC/EPSRC grant to WISB (BB/M017982/1), and China Postdoctoral Science Foundation (2017M623262).

Author contributions

WS, TL, YM and QW conceived and designed the experiments. TL, RF, YM, LL, LD, GF, WL and GH performed the experiments. MZ constructed the cDNA library. BMT designed the CAD7 mutants and surveyed the Avr3a-like effector family. PS, QW, YM and YD were involved in data interpretation and supported TL, BMT and WS in writing the manuscript. All authors reviewed the manuscript.

ORCID

Tingting Li  <https://orcid.org/0000-0002-5011-0174>
Patrick Schäfer  <https://orcid.org/0000-0002-0366-6858>
Weixing Shan  <https://orcid.org/0000-0001-7286-4041>
Brett M. Tyler  <https://orcid.org/0000-0003-1549-2987>
Qinhu Wang  <https://orcid.org/0000-0003-1251-073X>

References

- Anderson RG, Casady MS, Fee RA, Vaughan MM, Deb D, Fedkenheuer K, Huffaker A, Schmelz EA, Tyler BM, McDowell JM. 2012. Homologous RXLR effectors from *Hyaloperonospora arabidopsidis* and *Phytophthora sojae* suppress immunity in distantly related plants. *The Plant Journal* 72: 882–893.
- Armstrong MR, Whisson SC, Pritchard L, Bos JI, Venter E, Avrova AO, Rehmany AP, Bohme U, Brooks K, Cherevach I *et al.* 2005. An ancestral oomycete locus contains late blight avirulence gene *Avr3a*, encoding a protein that is recognized in the host cytoplasm. *Proceedings of the National Academy of Sciences, USA* 102: 7766–7771.
- Baxter A, Mittler R, Suzuki N. 2014. ROS as key players in plant stress signalling. *Journal of Experimental Botany* 65: 1229–1240.
- Boerjan W, Ralph J, Baucher M. 2003. Lignin biosynthesis. *Annual Review of Plant Biology* 54: 519–546.
- Boller T, He SY. 2009. Innate immunity in plants: an arms race between pattern recognition receptors in plants and effectors in microbial pathogens. *Science* 324: 742–744.
- Bomati EK, Noel JP. 2005. Structural and kinetic basis for substrate selectivity in *Populus tremuloides* sinapyl alcohol dehydrogenase. *Plant Cell* 17: 1598–1611.
- Bos JIB. 2007. Function, structure and evolution of the effector Avr3a of *Phytophthora infestans*. PhD Thesis, The Ohio State University, Columbus, OH.
- Bos JIB, Armstrong MR, Gilroy EM, Boevink PC, Hein I, Taylor RM, Tian ZD, Engelhardt S, Vetukuri RR, Harrower B *et al.* 2010. *Phytophthora infestans* effector AVR3a is essential for virulence and manipulates plant immunity by stabilizing host E3 ligase CMPG1. *Proceedings of the National Academy of Sciences, USA* 107: 9909–9914.
- Bos JIB, Kanneganti TD, Young C, Cakir C, Huitema E, Win J, Armstrong MR, Birch PR, Kamoun S. 2006. The C-terminal half of *Phytophthora infestans* RXLR effector AVR3a is sufficient to trigger R3a-mediated hypersensitivity and suppress INF1-induced cell death in *Nicotiana benthamiana*. *The Plant Journal* 48: 165–176.
- Boutemy LS, King SR, Win J, Hughes RK, Clarke TA, Blumenschein TM, Kamoun S, Banfield MJ. 2011. Structures of *Phytophthora* RXLR effector proteins: a conserved but adaptable fold underpins functional diversity. *Journal of Biological Chemistry* 286: 35834–35842.
- Chaparro-Garcia A, Schwizer S, Sklenar J, Yoshida K, Petre B, Bos JI, Schornack S, Jones AM, Bozkurt TO, Kamoun S. 2015. *Phytophthora infestans* RXLR-WY effector Avr3a associates with dynamin-related protein 2 required for endocytosis of the plant pattern recognition receptor FLS2. *PLoS ONE* 10: e0137071.
- Chaparro-Garcia A, Wilkinson RC, Gimenez-Ibanez S, Findlay K, Coffey MD, Zipfel C, Rathjen JP, Kamoun S, Schornack S. 2011. The receptor-like kinase SERK3/BAK1 is required for basal resistance against the late blight pathogen *Phytophthora infestans* in *Nicotiana benthamiana*. *PLoS ONE* 6: e16608.
- Costa MA, Collins RE, Anterola AM, Cochrane FC, Davin LB, Lewis NG. 2003. An *in silico* assessment of gene function and organization of the phenylpropanoid pathway metabolic networks in *Arabidopsis thaliana* and limitations thereof. *Phytochemistry* 64: 1097–1112.
- Dangl JL, Jones JD. 2001. Plant pathogens and integrated defence responses to infection. *Nature* 411: 826–833.
- Deb D, Anderson RG, How-Yew-Kin T, Tyler BM, McDowell JM. 2018. Conserved RXLR effectors from oomycetes *Hyaloperonospora arabidopsidis* and *Phytophthora sojae* suppress PAMP- and effector-triggered immunity in diverse plants. *Molecular Plant–Microbe Interactions* 31: 374–385.
- Dou DL, Kale SD, Wang XL, Chen YB, Wang QQ, Wang X, Jiang RHY, Arredondo FD, Anderson RG, Thakur PB *et al.* 2008. Conserved C-terminal motifs required for avirulence and suppression of cell death by *Phytophthora sojae* effector Avr1b. *Plant Cell* 20: 1118–1133.
- Fan G, Yang Y, Li T, Lu W, Du Y, Qiang X, Wen Q, Shan W. 2018. A *Phytophthora capsici* RXLR effector targets and inhibits a plant PPIase to suppress endoplasmic reticulum-mediated immunity. *Molecular Plant* 11: 1067–1083.
- Fernandez-Pozo N, Rosli HG, Martin GB, Mueller LA. 2015. The SGN VIGS tool: user-friendly software to design virus-induced gene silencing (VIGS) constructs for functional genomics. *Molecular Plant* 8: 486–488.
- Flor HH. 1971. Current status of the gene-for-gene concept. *Annual Review of Phytopathology* 9: 275–279.
- Gehl C, Waadt R, Kudla J, Mendel RR, Hansch R. 2009. New GATEWAY vectors for high throughput analyses of protein–protein interactions by bimolecular fluorescence complementation. *Molecular Plant* 2: 1051–1058.
- Gleave AP. 1992. A versatile binary vector system with a T-DNA organisational structure conducive to efficient integration of cloned DNA into the plant genome. *Plant Molecular Biology* 20: 1203–1207.

- Granke LL, Quesada-Ocampo L, Lamour K, Hausbeck MK. 2012. Advances in research on *Phytophthora capsici* on vegetable crops in the United States. *Plant Disease* 96: 1588–1600.
- Guindon S, Dufayard JF, Lefort V, Anisimova M, Hordijk W, Gascuel O. 2010. New algorithms and methods to estimate maximum-likelihood phylogenies: assessing the performance of PhyML 3.0. *Systematic Biology* 59: 307–321.
- Haas BJ, Kamoun S, Zody MC, Jiang RH, Handsaker RE, Cano LM, Grabherr M, Kodira CD, Raffaele S, Torto-Alalibo T *et al.* 2009. Genome sequence and analysis of the Irish potato famine pathogen *Phytophthora infestans*. *Nature* 461: 393–398.
- Hillmer RA, Tsuda K, Rallapalli G, Asai S, Truman W, Papke MD, Sakakibara H, Jones JDG, Myers CL, Katagiri F. 2017. The highly buffered Arabidopsis immune signaling network conceals the functions of its components. *PLoS Genetics* 13: e1006639.
- Ishihama N, Yamada R, Yoshioka M, Katou S, Yoshioka H. 2011. Phosphorylation of the *Nicotiana benthamiana* WRKY8 transcription factor by MAPK functions in the defense response. *Plant Cell* 23: 1153.
- Jiang RH, Tripathy S, Govers F, Tyler BM. 2008. RXLR effector reservoir in two *Phytophthora* species is dominated by a single rapidly evolving superfamily with more than 700 members. *Proceedings of the National Academy of Sciences, USA* 105: 4874–4879.
- Jones JD, Dangl JL. 2006. The plant immune system. *Nature* 444: 323–329.
- Kamoun S, Furrer O, Jones JD, Judelson HS, Ali GS, Dalio RJ, Roy SG, Schena L, Zambounis A, Panabieres F *et al.* 2015. The top 10 oomycete pathogens in molecular plant pathology. *Molecular Plant Pathology* 16: 413–434.
- Kiedrowski S, Kawalleck P, Hahlbrock K, Somssich IE, Dangl JL. 1992. Rapid activation of a novel plant defense gene is strictly dependent on the *Arabidopsis* RPM1 disease resistance locus. *EMBO Journal* 11: 4677–4684.
- Kim SJ, Kim MR, Bedgar DL, Moinuddin SG, Cardenas CL, Davin LB, Kang C, Lewis NG. 2004. Functional reclassification of the putative cinnamyl alcohol dehydrogenase multigene family in *Arabidopsis*. *Proceedings of the National Academy of Sciences, USA* 101: 1455–1460.
- Kim SJ, Kim KW, Cho MH, Franceschi VR, Davin LB, Lewis NG. 2007. Expression of cinnamyl alcohol dehydrogenases and their putative homologues during *Arabidopsis thaliana* growth and development: lessons for database annotations? *Phytochemistry* 68: 1957–1974.
- Kroon LP, Brouwer H, de Cock AW, Govers F. 2012. The genus *Phytophthora* anno 2012. *Phytopathology* 102: 348–364.
- Lamour KH, Stam R, Jupe J, Huitema E. 2012. The oomycete broad-host-range pathogen *Phytophthora capsici*. *Molecular Plant Pathology* 13: 329–337.
- Larkin MA, Blackshields G, Brown NP, Chenna R, McGettigan PA, McWilliam H, Valentin F, Wallace IM, Wilm A, Lopez R *et al.* 2007. Clustal W and Clustal X version 2.0. *Bioinformatics* 23: 2947–2948.
- Li L, Stoekert CJ Jr, Roos DS. 2003. OrthoMCL: identification of ortholog groups for eukaryotic genomes. *Genome Research* 13: 2178–2189.
- Liu YL, Schiff M, Marathe R, Dinesh-Kumar SP. 2002. Tobacco *Rar1*, *EDS1* and *NPR1/NIM1* like genes are required for N-mediated resistance to tobacco mosaic virus. *The Plant Journal* 30: 415–429.
- Luna E, Pastor V, Robert J, Flors V, Mauch-Mani B, Ton J. 2011. Callose deposition: a multifaceted plant defense response. *Molecular Plant–Microbe Interactions* 24: 183–193.
- Mackey D, Belkhadir Y, Alonso JM, Ecker JR, Dangl JL. 2003. *Arabidopsis* RIN4 is a target of the type III virulence effector AvrRpt2 and modulates RPS2-mediated resistance. *Cell* 112: 379–389.
- Mackey D, Holt BF, Wiig A, Dangl JL. 2002. RIN4 interacts with *Pseudomonas syringae* type III effector molecules and is required for RPM1-mediated resistance in *Arabidopsis*. *Cell* 108: 743–754.
- Mittler R. 2017. ROS are good. *Trends in Plant Science* 22: 11–19.
- Montesano M, Hyttiainen H, Wettstein R, Palva ET. 2003. A novel potato defence-related alcohol:NADP+ oxidoreductase induced in response to *Erwinia carotovora*. *Plant Molecular Biology* 52: 177–189.
- Mukhtar MS, Carvunis AR, Dreze M, Epple P, Steinbrenner J, Moore J, Tazan M, Galli M, Hao T, Nishimura MT *et al.* 2011. Independently evolved virulence effectors converge onto hubs in a plant immune system network. *Science* 333: 596–601.
- Rodriguez E, El Ghoul H, Mundy J, Petersen M. 2016. Making sense of plant autoimmunity and “negative regulators”. *FEBS Journal* 283: 1385–1391.
- Sang Y, Macho AP. 2017. Analysis of PAMP-triggered ROS burst in plant immunity. *Methods in Molecular Biology* 1578: 143–153.
- Schmelzer E, Kruger-Lebus S, Hahlbrock K. 1989. Temporal and spatial patterns of gene expression around sites of attempted fungal infection in parsley leaves. *Plant Cell* 1: 993–1001.
- Shan W, Cao M, Leung D, Tyler BM. 2004. The *Avr1b* locus of *Phytophthora sojae* encodes an elicitor and a regulator required for avirulence on soybean plants carrying resistance gene *Rps1b*. *Molecular Plant–Microbe Interactions* 17: 394–403.
- Sibout R, Eudes A, Mouille G, Pollet B, Lapierre C, Jouanin L, Seguin A. 2005. CINNAMYL ALCOHOL DEHYDROGENASE-C and -D are the primary genes involved in lignin biosynthesis in the floral stem of *Arabidopsis*. *Plant Cell* 17: 2059–2076.
- Somssich IE, Wernert P, Kiedrowski S, Hahlbrock K. 1996. *Arabidopsis thaliana* defense-related protein ELI3 is an aromatic alcohol:NADP(+) oxidoreductase. *Proceedings of the National Academy of Sciences, USA* 93: 14199–14203.
- Sun F, Kale SD, Azurmendi HF, Li D, Tyler BM, Capelluto DG. 2013. Structural basis for interactions of the *Phytophthora sojae* RxLR effector Avh5 with phosphatidylinositol 3-phosphate and for host cell entry. *Molecular Plant–Microbe Interactions* 26: 330–344.
- Trezzini GF, Horrichs A, Somssich IE. 1993. Isolation of putative defense-related genes from *Arabidopsis thaliana* and expression in fungal elicitor-treated cells. *Plant Molecular Biology* 21: 385–389.
- Tronchet M, Balague C, Kroj T, Jouanin L, Roby D. 2010. Cinnamyl alcohol dehydrogenases-C and D, key enzymes in lignin biosynthesis, play an essential role in disease resistance in *Arabidopsis*. *Molecular Plant Pathology* 11: 83–92.
- Tyler BM. 2001. Genetics and genomics of the oomycete-host interface. *Trends in Genetics* 17: 611–614.
- Tyler BM. 2017. The fog of war: how network buffering protects plants’ defense secrets from pathogens. *PLoS Genetics* 13: e1006713.
- Varbanova M, Porter K, Lu F, Ralph J, Hammerschmidt R, Jones AD, Day B. 2011. Molecular and biochemical basis for stress-induced accumulation of free and bound p-coumaraldehyde in cucumber. *Plant Physiology* 157: 1056–1066.
- Vega-Arreguin JC, Jalloh A, Bos JI, Moffett P. 2014. Recognition of an Avr3a homologue plays a major role in mediating nonhost resistance to *Phytophthora capsici* in *Nicotiana* species. *Molecular Plant–Microbe Interactions* 27: 770–780.
- Wallace IM, O’Sullivan O, Higgins DG, Notredame C. 2006. M-Coffee: combining multiple sequence alignment methods with T-Coffee. *Nucleic Acids Research* 34: 1692–1699.
- Wang X, Boevink P, McLellan H, Armstrong M, Bukharova T, Qin Z, Birch PR. 2015. A host KH RNA-binding protein is a susceptibility factor targeted by an RXLR effector to promote late blight disease. *Molecular Plant* 8: 1385–1395.
- Wang QQ, Han CZ, Ferreira AO, Yu XL, Ye WW, Tripathy S, Kale SD, Gu BA, Sheng YT, Sui YY *et al.* 2011. Transcriptional programming and functional interactions within the *Phytophthora sojae* RXLR effector repertoire. *Plant Cell* 23: 2064–2086.
- Wang Y, Wang Y. 2018. Trick or treat: microbial pathogens evolved apoplastic effectors modulating plant susceptibility to infection. *Molecular Plant–Microbe Interactions* 31: 6–12.
- Wang Y, Xu Y, Sun Y, Wang H, Qi J, Wan B, Ye W, Lin Y, Shao Y, Dong S *et al.* 2018. Leucine-rich repeat receptor-like gene screen reveals that *Nicotiana* RXEG1 regulates glycoside hydrolase 12 MAMP detection. *Nature Communications* 9: 594.
- Win J, Krasileva KV, Kamoun S, Shirasu K, Staskawicz BJ, Banfield MJ. 2012. Sequence divergent RXLR effectors share a structural fold conserved across plant pathogenic oomycete species. *PLoS Pathogens* 8: e1002400.
- de Wit PJ. 2016. *Cladosporium fulvum* effectors: weapons in the arms race with tomato. *Annual Review of Phytopathology* 54: 1–23.
- Yaeno T, Li H, Chaparro-Garcia A, Schornack S, Koshiba S, Watanabe S, Kigawa T, Kamoun S, Shirasu K. 2011. Phosphatidylinositol monophosphate-binding interface in the oomycete RXLR effector AVR3a is required for its stability in host cells to modulate plant immunity. *Proceedings of the National Academy of Sciences, USA* 108: 14682–14687.
- Yoo SD, Cho YH, Sheen J. 2007. *Arabidopsis* mesophyll protoplasts: a versatile cell system for transient gene expression analysis. *Nature Protocols* 2: 1565–1572.

- Youn B, Camacho R, Moinuddin SG, Lee C, Davin LB, Lewis NG, Kang C. 2006. Crystal structures and catalytic mechanism of the *Arabidopsis* cinnamyl alcohol dehydrogenases AtCAD5 and AtCAD4. *Organic & Biomolecular Chemistry* 4: 1687–1697.
- Zhang X, Henriques R, Lin SS, Niu QW, Chua NH. 2006. *Agrobacterium*-mediated transformation of *Arabidopsis thaliana* using the floral dip method. *Nature Protocols* 1: 641–646.
- Zheng Z, Qamar SA, Chen Z, Mengiste T. 2006. Arabidopsis WRKY33 transcription factor is required for resistance to necrotrophic fungal pathogens. *The Plant Journal* 48: 592–605.

Supporting Information

Additional Supporting Information may be found online in the Supporting Information section at the end of the article.

Dataset S1 The Avr3a-like sequences identified in this study.

Dataset S2 The CAD homologs identified in this study.

Fig. S1 Arrangement of PcAvr3a-like genes in the LT263 genome.

Fig. S2 Transcript levels of PcAvr3a-like effect genes during infection of *Arabidopsis thaliana* and *Nicotiana benthamiana*.

Fig. S3 Residues conserved among Avr3a-like effectors used in this study.

Fig. S4 Immunodetection of proteins from *N. benthamiana* expressing BiFC constructs.

Fig. S5 Phylogenetic analysis of the plant CAD family proteins.

Fig. S6 *AtCAD7*, *AtCAD6* and *AtCAD8* are induced during *P. capsici* infection.

Fig. S7 Interaction of AtCAD6 and AtCAD8 with Avr3a-like effectors.

Fig. S8 Co-localization analysis of CAD7 and effectors.

Fig. S9 Expression of CAD genes in CAD7-silenced plants.

Fig. S10 Morphology of *AtCAD7*-silenced *Arabidopsis* plants (Ri) (a), virus induced *NbCAD7* silenced *N. benthamiana* plants TRV::*NbCAD7* (tNb7) (b), and transgenic *AtCAD7* (OE7) or *AtCAD7m* (OE7m) *Arabidopsis* plants (c).

Fig. S11 Over-expression of *NbCAD7* does not promote *P. capsici* infection.

Fig. S12 Amino acid sequence alignment of AtCAD7, AtCAD5 and PtSAD.

Fig. S13 Histochemical analysis of lignified tissues of *AtCAD7* silenced plants (Ri), *AtCAD7* overexpression plants OE7 and *AtCAD7m* transgenic plants OE7m.

Fig. S14 Wild-type and mutant AtCAD7 proteins could suppress INF1-triggered cell death.

Fig. S15 The expression of defense-related genes in *AtCAD7*-overexpressing *Arabidopsis* plants.

Fig. S16 AtCAD7 is stabilized by Avr3a-like effectors in *Arabidopsis* protoplasts.

Fig. S17 NbCMPG1 proteins are not bound by NbCAD7 nor by PcAvr3a12.

Table S1 Primers used in this study.

Please note: Wiley Blackwell are not responsible for the content or functionality of any Supporting Information supplied by the authors. Any queries (other than missing material) should be directed to the *New Phytologist* Central Office.